Next Generation Weather Radar

Automatic Detection of Mesocyclonic Shear Test Results

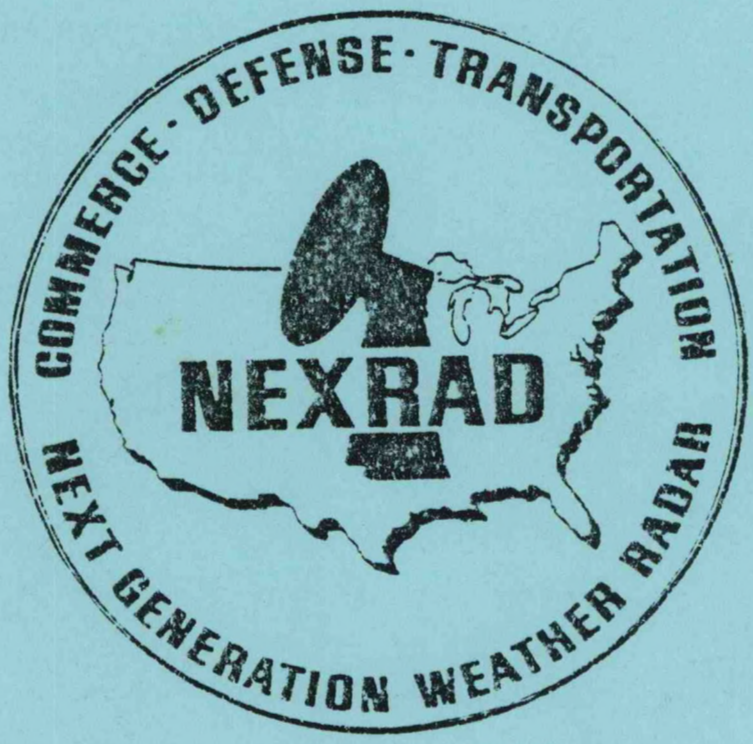

January 1984

Prepared for

The NEXRAD Joint System Program Office

AUTOMATIC DETECTION OF MESOCYCLONIC SHEAR TEST RESULTS

Dusan S. Zrnic', D.W. Burgess, and Y. Gal-Chen*

National Severe Storms Laboratory
1313 Halley Circle
Norman, OK 73069

*Cooperative Institute for Mesoscale Meteorological Studies, University of Oklahoma, Norman, OK 73019

TABLE OF CONTENTS

TABLES

LIST OF FIGURES

ABSTRACT

We report results of studies of an algorithm that detects mesocyclonic shear in storms. Large intense tornadoes are always spawned in regions of high shear. The algorithm uses decision thresholds to discriminate between mesocyclonic and other shears not associated with organized circulatory flow. We have observed that distant mesocyclonic features become elongated in the beam's azimuthal direction. Thus, asymmetry criterion that checks the radial and azimuthal extent of the mesocyclone are range dependent. Data from sixteen mesocyclones were subjected to the algorithm. For these data the probability of false alarm per storm cell is 10%, and the probability of detection is 90%.

1. Introduction

The purpose of this report is to document the performance evaluation of the mesocyclone detection algorithm developed for Next Generation Weather Radar (NEXRAD) use. A detailed description of the algorithm is presented in Hennington and Burgess (1981) as well as in the NEXRAD algorithm report (1983) and hence will not be repeated here; rather, additions and changes will be explained as well as the reason for choosing particular thresholds that discriminate between shears and mesocyclones. Altnough we have obtained a good idea about the effectiveness of our algorithm on several hours of Doppler data, collected in a variety of situations, we are not sure how the program will react in all circumstances.

The development process consisted of examining the data after each run and adjusting the algorithm accordingly. It took several iterations to adapt the method so that it would work satisfactorily on all the cases studied up to that point. That, however, does not guarantee a similar performance on a different data set. Yet, by choosing a variety of storms with mesocyclones, at various stages of maturity and at several ranges from the radar, we hoped to exhaust the "usual" possibilities. We also ran the algorithm on data that did not contain circulations. Overall, however, we have tested it only on the Oklahoma variety of isolated, supercell-type storms and squall lines.

2. Detection Thresholds

To give the reader an appreciation of the complexity of the problem, we list in Table 1 and discuss below the variables that influence the performance of our algorithm. These are mostly thresholds used to classify some attribute of either a pattern vector or a feature (Zrnic' et al., 1982). Obviously there are many variables, each of which can take a continuum of values, and a good part of our endeavor was spent in identifying the values that would ensure best performance.

2.1 Momentum and Shear Thresholds

Because our detection algorithm relies heavily on mesocyclonic properties (i.e., shear and momentum), we present here some statistical data concerning these quantities that influenced the choices in Table 1. An exhaustive search through 1977 single-Doppler data by JDOP staff (1979) revealed 40

TABLE 1

List of Thresholds on Variables

Threshold		Numerical Values
L_s	Low shear	2 $m \cdot s^{-1} \cdot km^{-1}$
H_s	High shear	4 $m \cdot s^{-1} \cdot km^{-1}$
L_m	Low momentum	50 $m \cdot s^{-1} \cdot km^{-1}$
H_m	High momentum	150 $m \cdot s^{-1} \cdot km^{-1}$
D_1/D_r	First ratio of feature lengths	0.5 to 2
D_2/D_r	Second ratio of feature lengths	0.5 to 2
D_3/D_r	Third ratio of feature lengths	1.6 to 4
M	Minimum number of vectors allowed in a feature	6
R	Maximum distance between the azimuthal centers of two vectors for classification in the same feature	2.2°
N	Maximum radial distance between two vectors	1 km
CV	Threshold for the average sum of beginning and ending velocities in a feature	18 $m \cdot s^{-1}$
RTH	Reflectivity threshold	15 dBZ

mesocyclones. The shear values for these mesocyclones are reproduced on Figure 1; they were not obtained at the time of first detection but somewhat later. Note the decreasing trend with range, which is due to smoothing by the beamwidth and a large scatter difficult to accommodate with range-dependent thresholds. The solid line L_S indicates the low shear threshold of 2 $m \cdot s^{-1} \cdot km^{-1}$ used by our algorithm; this ensures that no vector associated with mesocyclone core is missed in any of these mesocyclones. Importantly, Burgess (1976) shows that background shear in nonmesocyclonic storms is below 2 $m \cdot s^{-1} \cdot km^{-1}$. For these reasons we expect the probability of detection to be close to 1 and false alarms to be rare. The high shear threshold of 4 $m \cdot s^{-1} \cdot km^{-1}$ on the same figure indicates that some mesocyclonic shears might be missed if it were not for two momentum thresholds that also influence the detection process.

Measured momentum defined by a product of maximum velocity difference Δv with the diameter D for the same data set is plotted on Figure 2. There is no visible range dependence, although the least squares fit suggests a slight increase with range. This could be partly due to the smoothing by the beam so that further vortices appear to have larger diameters. But the low momentum threshold of 50 $m \cdot s^{-1} \cdot km^{-1}$ ensures that no mesocyclone from these data is below it.

The detection region in the shear momentum plane was examined for these data in order to determine suitable high thresholds (Fig. 3). We see that only one tornadic mesocyclone is lost with the high threshold of 4 $m \cdot s^{-1} \cdot km^{-1}$ for shear and 150 $m \cdot s^{-1} \cdot km$ for momentum. But this mesocyclone was at 300 km, which is 80 km beyond stipulated requirements for NEXRAD. At such distance, beamwidth resolution and azimuthal sampling are inadequate to resolve but the most intense mesocyclones.

Observe that the high momentum threshold could be increased to 275 $m \cdot s^{-1} \cdot km$ without losing additional mesocyclones in the data set; the high shear threshold remains at 4 $m \cdot s^{-1} \cdot km^{-1}$. We have adopted a more conservative approach, wherein $H_m = 3L_m$ and $H_S = 2L_S$, until we learn more about these from other data.

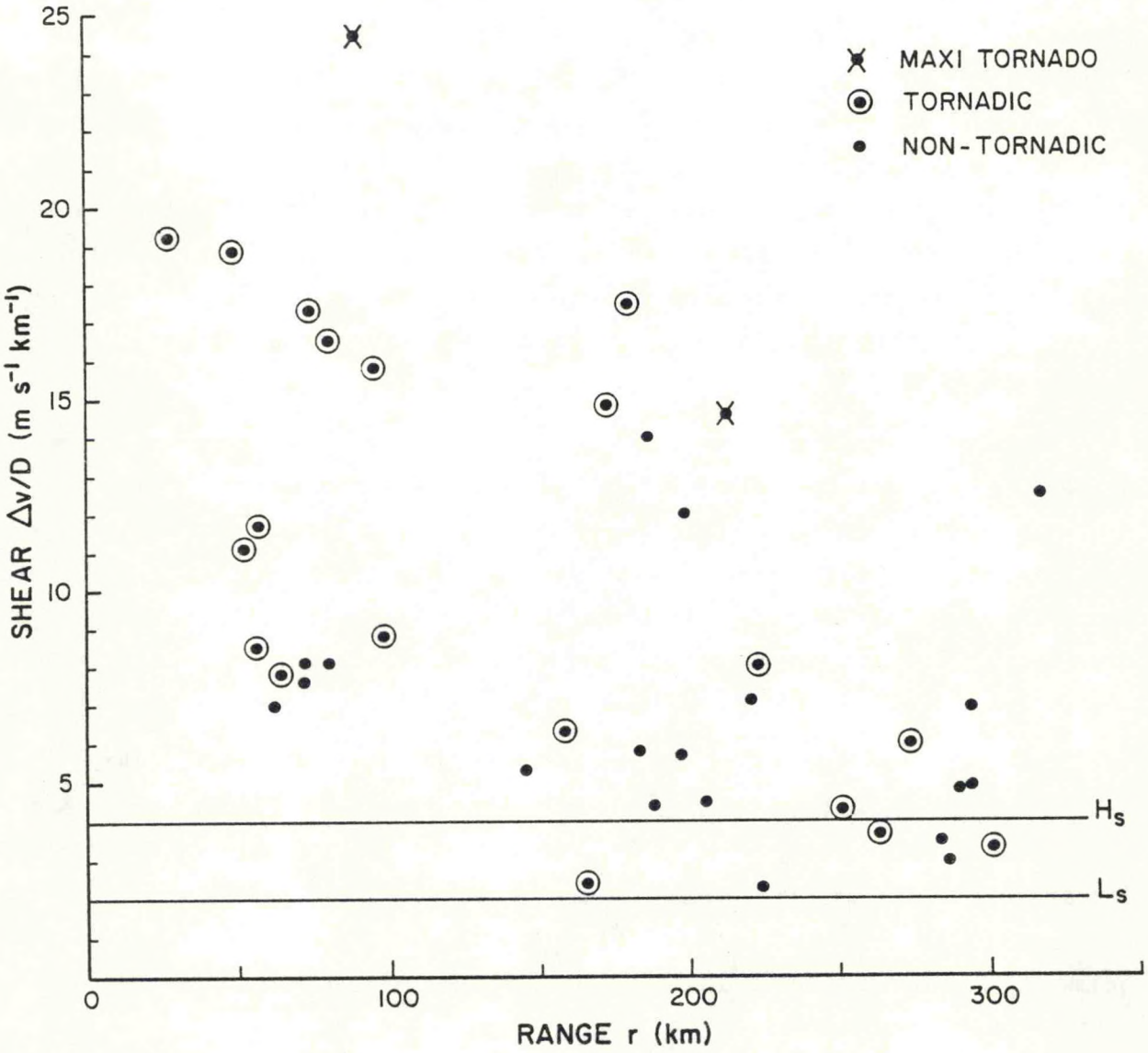

Figure 1: Shear versus range for 40 mesocyclones observed by the Norman Doppler radar during the spring of 1977. Low shear and high shear thresholds used by our algorithm are indicated.

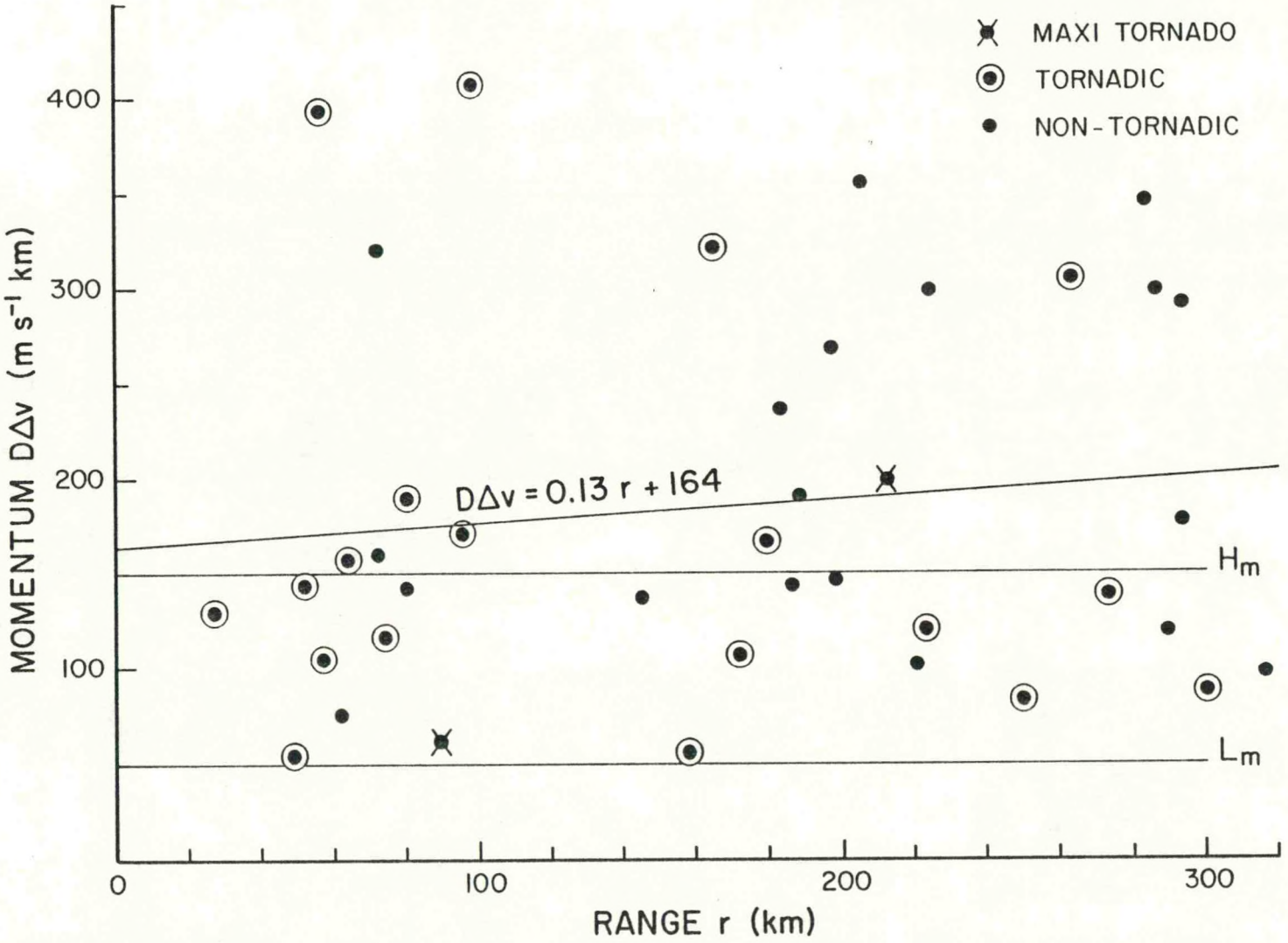

Figure 2: Momentum versus range for the same mesocyclones as on Fig. 1. A least squares fitted straight line is also drawn. Low and high momentum thresholds are drawn.

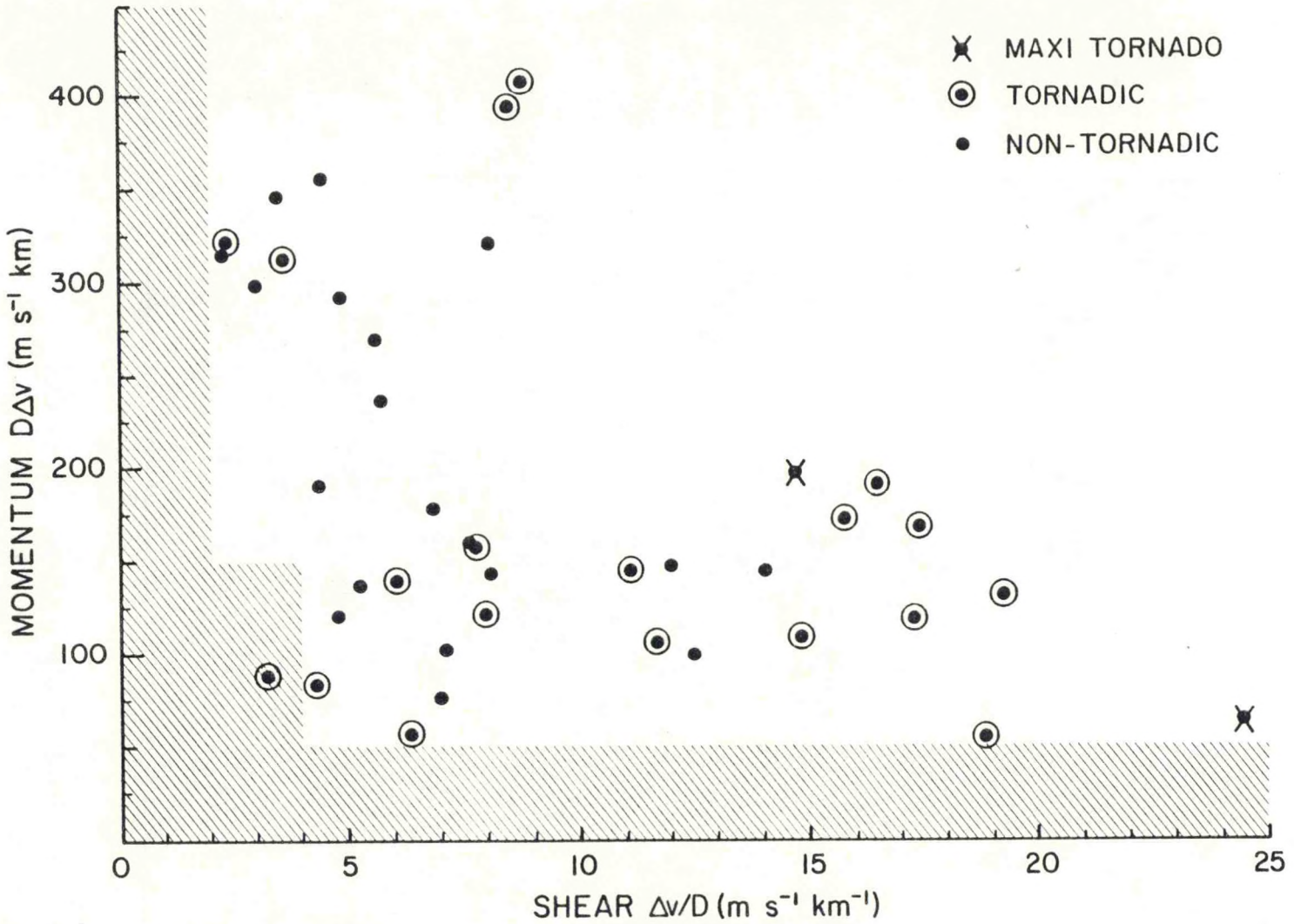

Figure 3: Momentum versus shear from Fig. 1 and Fig. 2. The detection region for our thresholds is indicated.

2.2 Other Threshold Variables

To reduce localized transient phenomena, a feature must contain at least six vectors before it can be classified as a shear (S) or mesocylonic shear (M). With range gate spacings of 1 μs, this corresponds to a minimum range extent of 900 m. Since the minimum mesocyclone diameter in our data is 1.6 km (Fig. 4), we see that up to 45% of the area of such a small mesocyclone could be masked with range-overlaid echoes or lost because of some other cause, but the algorithm would still consider it.

The maximum allowed separation between the centers of two adjacent vectors must be such that the radial separation is less than 1 km and the azimuth separation less than 2.2°. The 1-km distance in range is again taken from considerations of small diameters (~2 km) so that if there is a 1-km gap in data, such small mesocyclone would still be recognized. The azimuthal separation is dictated by the radial spacing, which is about 1°, so that 2.2° allows one or two missed radials.

2.3 Symmetry Criteria

The magnitude of the average of beginning and ending velocities in a feature is checked against an 18 $m \cdot s^{-1}$ threshold. If it is exceeded, the imbalance is considered large and the feature is classified as shear. This value was determined empirically from several data sets. We emphasize that such a "balance of velocities" threshold is applicable only if the mesocyclone (storm) motion has been removed from the radial components of velocities. This removal is highly recommended because it reduces aliasing and facilitates mesocyclone recognition by people and machines.

Since the mesocyclone can be well approximated with a Rankine combined model, we set out to detect its solidly rotating core (Zrnic' et al., 1982). However, after examining the shapes of features that had been detected, it became apparent that a considerable portion of the mesocyclone outside a rotating core was part of the feature. Examination of the isodops of a Rankine model vortex reveals that a region delineated with heavy lines (Fig. 5) is the envelope of the pattern vectors. We shall show that the extent of this region in range (y direction) depends on the shear threshold. We start by noting that the line parallel to the x axis connecting $y = -x$ with $y = x$ has length

$$\Delta = \frac{v_m r_t}{v_r} \tag{1}$$

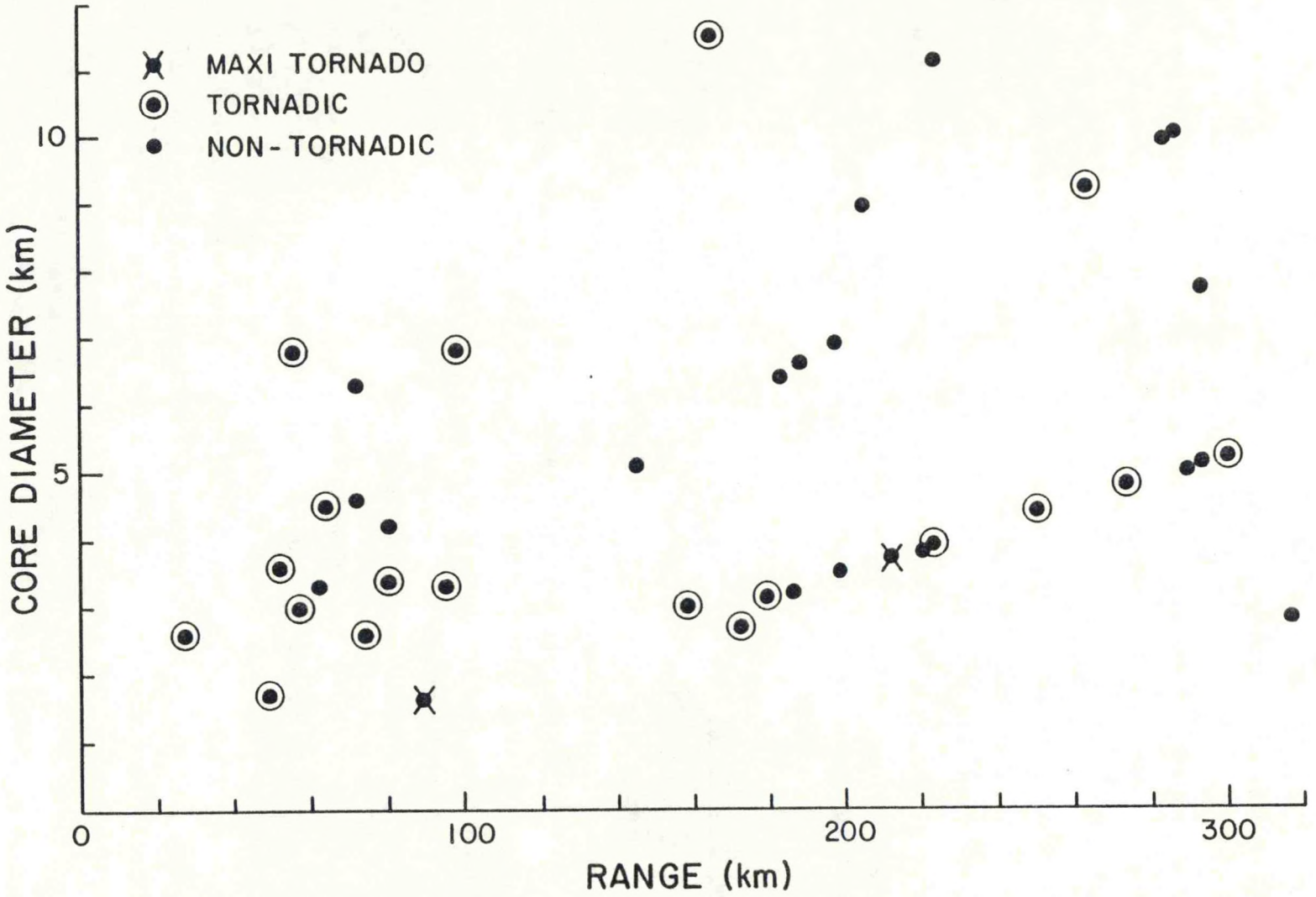

Figure 4: Estimated diameters for the mesocyclones whose shears are on Fig. 1.

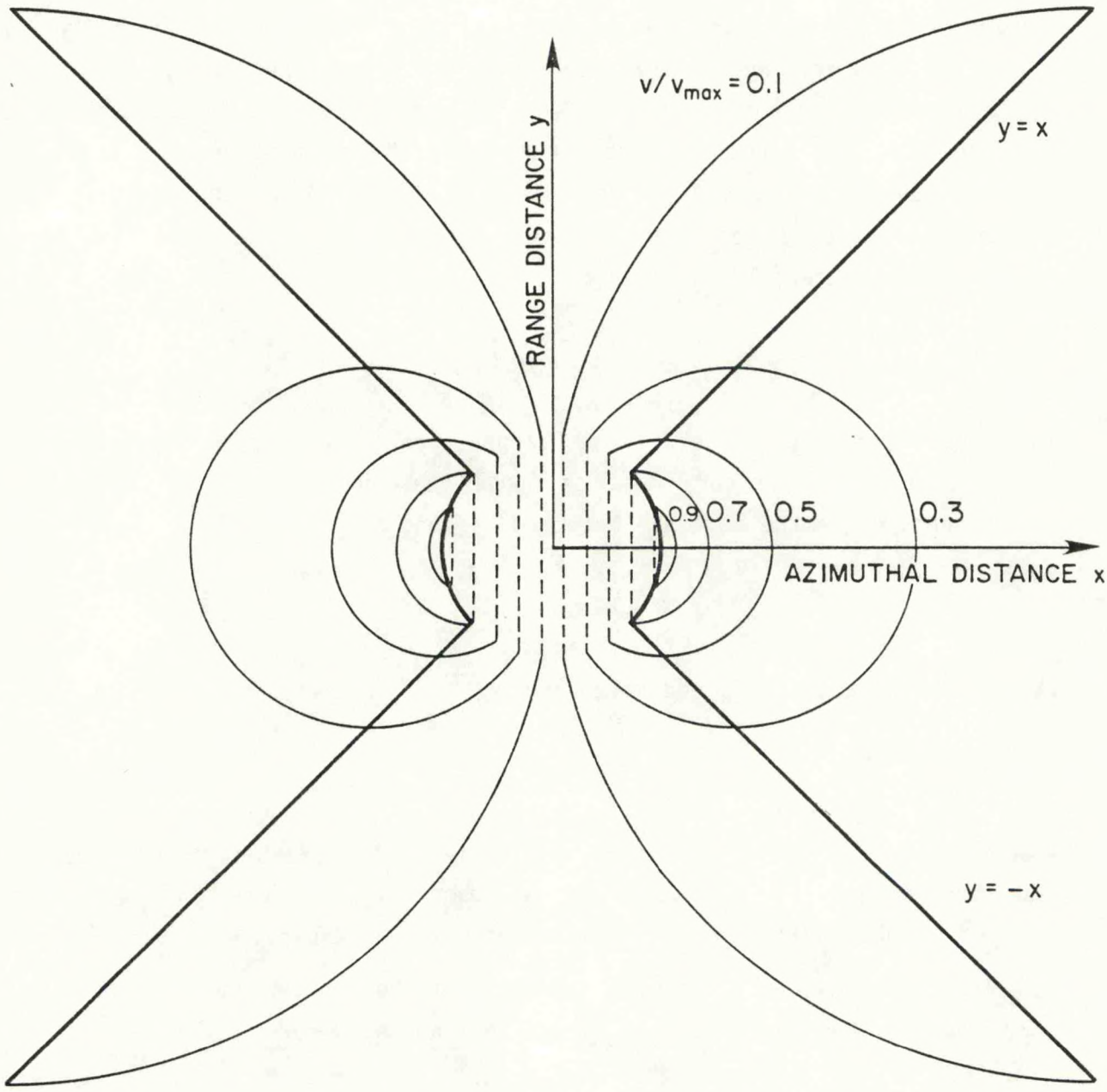

Figure 5: Envelope of pattern vectors (thick lines) for an ideal Rankine vortex observed by a Doppler radar with perfect resolution.

where v_m = maximum tangential velocity; r_t is vortex radius; and v_r is a radial velocity, at a particular point y=x. The "momentum" (estimated by the algorithm) outside the solidly rotating core is constant $2v_m r_t$. This is $1/2$ of the actual momentum of the solidly rotating core and is independent of the distance from the core. Let us assume that the mesocyclone has sufficient momentum ($4v_m r_t$) so that $2v_m r_t$ is above the high momentum thresholds. Thus, the detection depends only on the shear threshold L_s (Fig. 3). Also assume that the shear threshold is given by

$$L_s = v_m/kr_t \tag{2}$$

where the shear factor k is a number larger than 1, because we assume that the shear centered on the core must be above the threshold. Then the pattern vectors outside of the core are detected as long as

$$2v_r/\Delta > L_s, \tag{3}$$

which with (1) and (2) is equivalent to

$$v_r > v_m/\sqrt{2k}. \tag{4}$$

However, if the pattern vectors fail the high momentum threshold, then detection depends on H_s only and we can use the same analysis, i.e., $H_s=v_m/kr_t$, that would lead to identical normalized results.

The radial extent D_r (radial diameter) of the mesocyclone depends also on L_s. Since on the line y=x, $v_r=v_m r_t/2y$, we find the shear

$$2v_r/y = v_m r_t/2y^2. \tag{5}$$

Equating (5) to L_s, we obtain

$$D_r = \lessdot 2y = \sqrt{\frac{2v_m r_t}{L_s}} = r_t\sqrt{2k} \tag{6}$$

The azimuthal extent (diameter) is calculated using three methods. First, a momentum weighted diameter is

$$D_1 = \Sigma\Delta_i^2 v_i / \Sigma\Delta_i v_i \tag{7}$$

where Δ_i is the azimuthal length of a velocity run (pattern vector), and v_i is the difference between ending and beginning velocities.

The second diameter D_2 comes from the square of Δ_i,

$$D_2 = \Sigma\Delta_i^2 / \Sigma\Delta_i, \tag{8}$$

and the third is a simple average,

$$D_3 = \Sigma\Delta_i / M, \tag{9}$$

where M is the number of pattern vectors in a feature. After replacing (7), (8) and (9) with integrals, and for an ideal mesocyclone signature, one obtains

$$D_1 = \left[\int_0^b (2x)^2 v_m \cos\theta\, dy + \int_b^{y_m} 2y v_m r_t\, dy\right] / \left[\int_0^b 2x v_m \cos\theta\, dy + \int_b^{y_m} v_m r_t\, dy\right] \tag{10}$$

$$D_2 = \left[\int_0^b (2x)^2 dy + \int_b^{y_m} (2y)^2 dy\right] / \left[\int_0^b 2x\, dy + \int_b^{y_m} 2y\, dy\right] \tag{11}$$

$$D_3 = \left[\int_0^b 2x\, dy + \int_b^{y_m} 2y\, dy\right] / \int_0^{y_m} dy \tag{12}$$

where $b = r_t / \sqrt{2}$ and $x = r_t \cos\theta$. Equations (10), (11) and (12) are valid for an ideal Rankine combined model vortex. Furthermore, it implicitly assumed that the azimuthal resolution is much finer than the vortex radius. Under these conditions, integration of (10), (11) and (12) produces

$$D_1 = 2r_t(3\pi/8 + 0.5 + k/2)/(5\sqrt{2/3} + \sqrt{2k} - \sqrt{2}) \quad (13)$$

$$D_2 = 2r_t(10\sqrt{2/3} + 2^{3/2}k^{3/2}/3 - 2^{3/2}/3)/(\pi + 2k) \quad (14)$$

$$D_3 = 2r_t(\pi/8 - 0.25 + k/2)/\sqrt{2k} \quad (15)$$

Our original criterion that classified features into mesocyclonic shear (M) or shear (S) used a logical check such that

$$IF((0.5 < \hat{D}_{1e}/\hat{D}_r < 2) \text{ OR } (0.5 < \hat{D}_{2e}/\hat{D}_r < 2)) \quad (16)$$

was satisfied the feature was declared a mesocyclonic shear. The ^ over the variables denotes the estimated (radar measured) distances (Zrnic' et al., 1982), and $\hat{D}_{1e}$ and $\hat{D}_{2e}$ are corrected estimates of the azimuthal lengths:

$$\hat{D}_{1e} = \frac{3\pi}{8}\hat{D}_1 \quad (17)$$

$$\hat{D}_{2e} = \frac{4}{\pi}\hat{D}_2. \quad (18)$$

These corrections really should depend on the range of the mesocyclone and on the shear factor k. Dependence on k is strongest for small values of k as seen in Fig. 6 where the ratios D_1/D_r are plotted. From the data on Fig. 1, $k = \Delta v/L_s D$, we find minimum k of 1.2 and maximum 12, but past the value of 12 the ratios are almost constant. Therefore, for larger values of k, we can use constant multiplying factors (about 2 for D_1 and 1.5 for D_2). But then for lower values of k, the mesocyclone would fail our symmetry criterion. Also we found that at distant ranges azimuthal lengths tend to be larger than radial lengths, which is strictly due to beam smoothing (see appendix A). So we left the criterion (16) and added to it a further symmetry

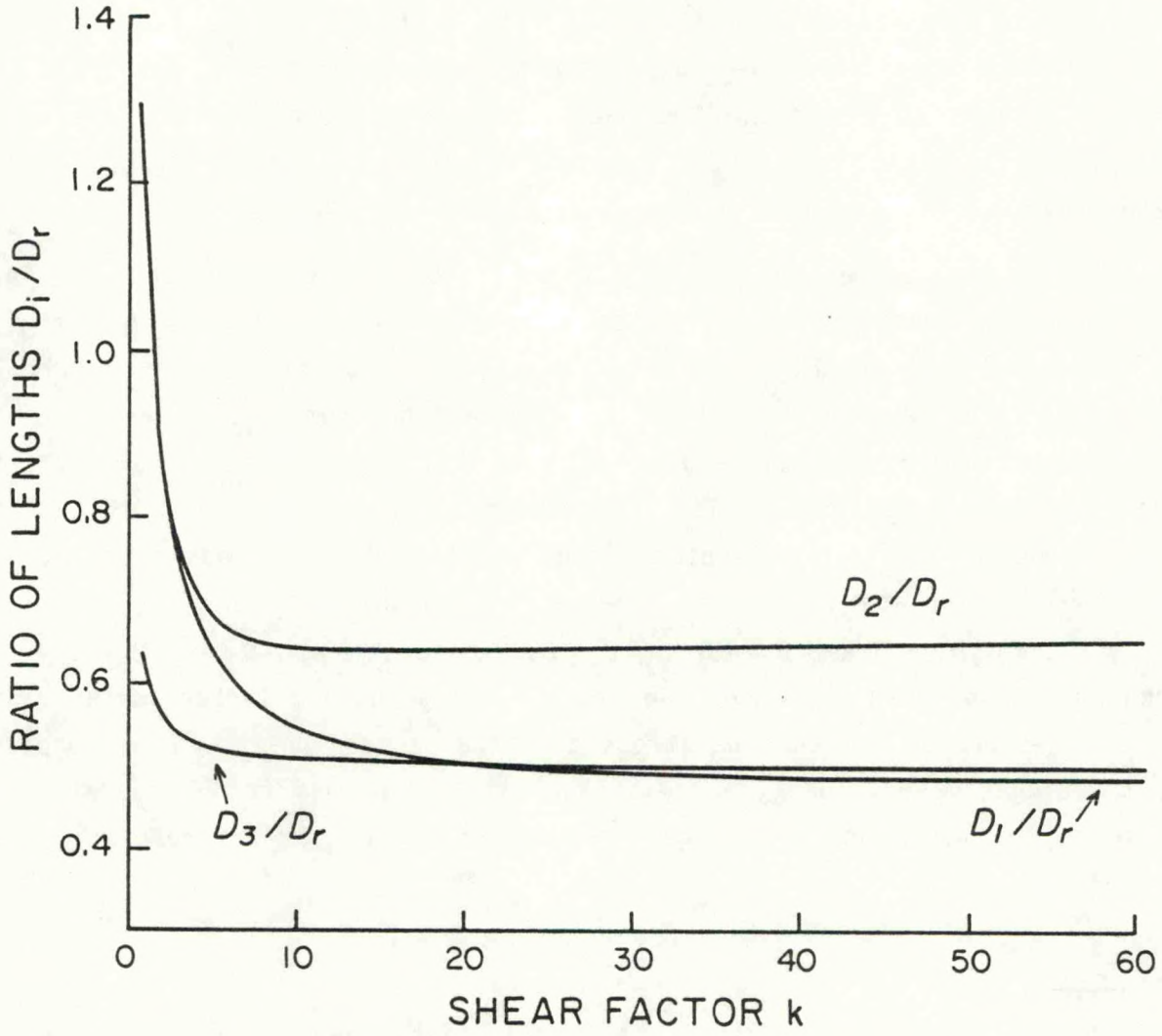

Figure 6: Ratios of azimuthal to radial length versus the shear factor k.

check applicable at ranges larger than 140 km. The check

$$IF(0.8 \leq \hat{D}_3/2\hat{D}_r \leq 2) \qquad (19)$$

is in an OR combination with (16) (but only at ranges beyond 140 km). This addition was made after we failed to properly classify a mesocyclone at 150 km. Prior to the change we had a zero (0) probability of false alarm (P_{fa}) per cell for the particular two volume scans and a probability of detection (P_d) of only 0.66 (see next section).

To illustrate the applicability of our calculations, we present on Fig. 7 the feature of pattern vectors in an azimuth range plot that is very similar to the ideal one on Fig. 5. From detailed analysis and photographs, we estimate at low levels (below 1 km) r_t = 450 m, and from Fig. 7, we deduce the measured maximum rotational velocity v_m = 48 $m \cdot s^{-1}$; therefore we calculate the shear factor k (2) to be 53. The calculated radial extent (6) of the mesocyclone becomes 4.5 km, which agrees exactly with the measured one. The azimuthal calculated and measured lengths are as follows: D_1 = 2.2 km, $\hat{D}_1$ = 3 km; D_2 = 3 km, $\hat{D}_2$= 3.3 km, D_3 = 2 km, $\hat{D}_3$ = 2.8 km. This good agreement would have been even better had we used a larger vortex radius at this height of 1.6 km. We stress that the pattern on Fig. 7 was produced by the Binger mesocyclone (see next section), which was strong and relatively close to the radar where the idealized assumption of perfect resolution is a good approximation.

3. Tests:

Over the last several years, NSSL scientists have compiled considerable amounts of data on mesocyclones from Doppler radar observation. Thus, our understanding of the phenomenon has progressed, yet it is very difficult to translate this understanding into an automatic procedure for detection. Furthermore, it is not clear how best to compute the probability of false alarm and that of detection. Therefore, a certain degree of arbitrariness is necessary. Before we are ready to proceed with a true detection of mesocyclones (using height and time continuity), we need to assess how the algorithm performs at a single height in storms with and without mesocyclones. Thus, we seek the probability of false alarm per storm cell P_{fa} and the detection probability P_d. A cell is defined with a 30 dBZ

EXAMPLE ONE

TAPE: 0991-197 TIME:193949-191005

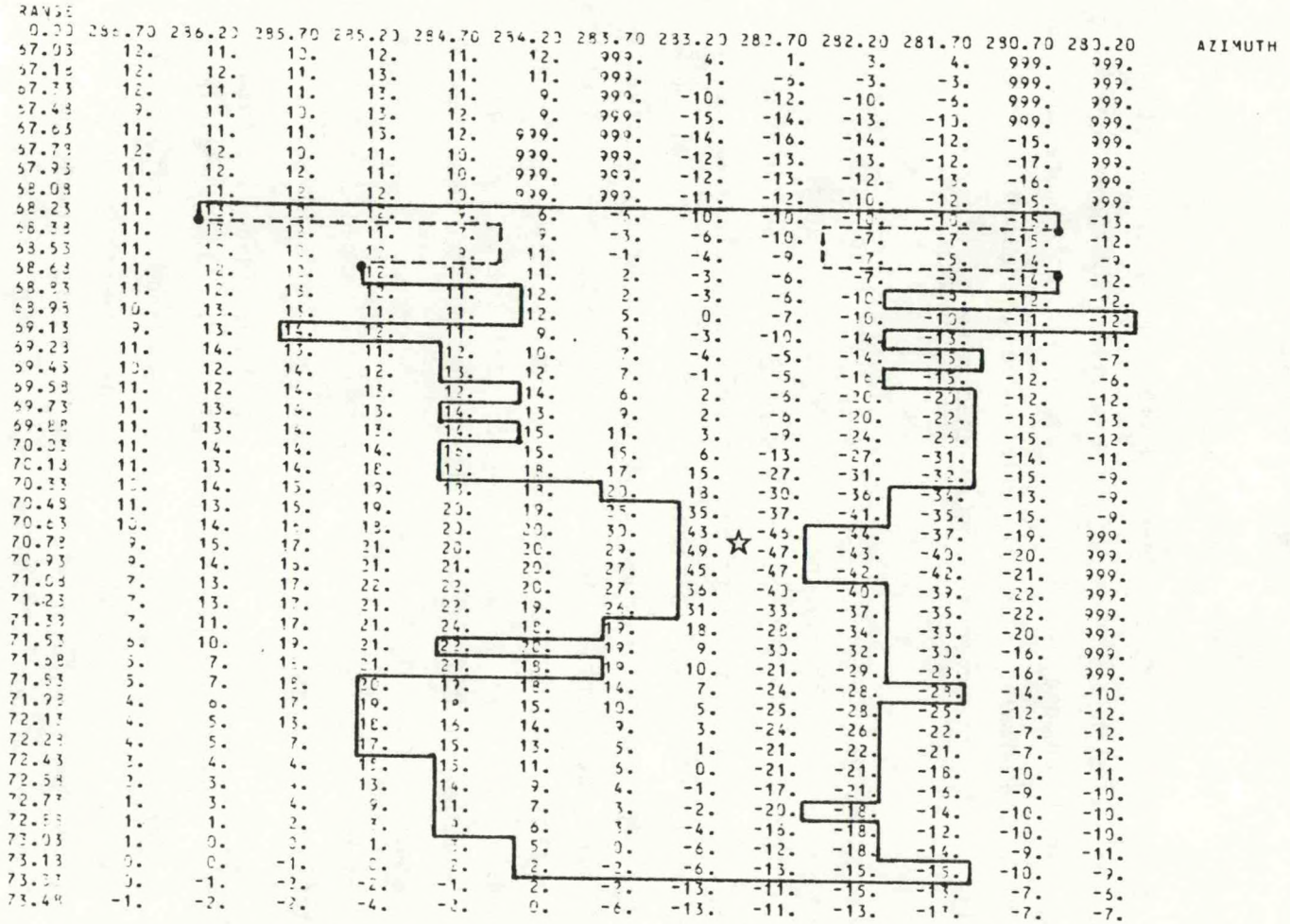

RANGE	286.70	286.20	285.70	285.20	284.70	284.20	283.70	283.20	282.70	282.20	281.70	280.70	280.20	AZIMUTH
67.03	12.	11.	10.	12.	11.	12.	999.	4.	1.	3.	4.	999.	999.	
67.18	12.	12.	11.	13.	11.	11.	999.	1.	-5.	-3.	-3.	999.	999.	
67.33	12.	11.	11.	13.	11.	9.	999.	-10.	-12.	-10.	-6.	999.	999.	
67.48	9.	11.	10.	13.	12.	9.	999.	-15.	-14.	-13.	-10.	999.	999.	
67.63	11.	11.	11.	13.	12.	999.	999.	-14.	-16.	-14.	-12.	-15.	999.	
67.78	12.	12.	10.	11.	10.	999.	999.	-12.	-13.	-13.	-12.	-17.	999.	
67.93	11.	12.	12.	11.	10.	999.	999.	-12.	-13.	-12.	-13.	-16.	999.	
68.08	11.	11.	12.	12.	10.	999.	999.	-11.	-13.	-10.	-12.	-15.	999.	
68.23	11.	11.	12.	12.	9.	6.	-6.	-10.	-10.	-10.	-10.	-15.	-13.	
68.38	11.	12.	12.	11.	9.	9.	-3.	-6.	-10.	-7.	-7.	-15.	-12.	
68.53	11.	12.	12.	12.	9.	11.	-1.	-4.	-9.	-7.	-5.	-14.	-9.	
68.68	11.	12.	12.	12.	11.	11.	2.	-3.	-6.	-7.	-9.	-14.	-12.	
68.83	11.	12.	13.	12.	11.	12.	2.	-3.	-6.	-10.	-9.	-12.	-12.	
68.98	10.	13.	13.	11.	11.	12.	5.	0.	-7.	-10.	-10.	-11.	-12.	
69.13	9.	13.	13.	12.	11.	9.	5.	-3.	-10.	-14.	-13.	-11.	-11.	
69.28	11.	14.	13.	11.	12.	10.	7.	-4.	-5.	-14.	-13.	-11.	-7.	
69.43	10.	12.	14.	12.	13.	12.	7.	-1.	-5.	-16.	-15.	-12.	-6.	
69.58	11.	12.	14.	13.	12.	14.	6.	2.	-6.	-20.	-20.	-12.	-12.	
69.73	11.	13.	14.	13.	14.	13.	9.	2.	-6.	-20.	-22.	-15.	-13.	
69.88	11.	13.	14.	13.	14.	15.	11.	3.	-9.	-24.	-26.	-15.	-12.	
70.03	11.	14.	14.	14.	16.	15.	15.	6.	-13.	-27.	-31.	-14.	-11.	
70.18	11.	13.	14.	16.	16.	18.	17.	15.	-27.	-31.	-32.	-15.	-9.	
70.33	10.	14.	15.	19.	19.	19.	20.	18.	-30.	-36.	-34.	-13.	-9.	
70.48	11.	13.	15.	19.	20.	19.	25.	35.	-37.	-41.	-35.	-15.	-9.	
70.63	10.	14.	16.	18.	20.	20.	30.	43.	-45.	-44.	-37.	-19.	999.	
70.78	9.	15.	17.	21.	20.	20.	29.	49.	-47.	-43.	-40.	-20.	999.	
70.93	9.	14.	16.	21.	21.	20.	27.	45.	-47.	-42.	-42.	-21.	999.	
71.08	7.	13.	17.	22.	22.	20.	27.	36.	-40.	-40.	-39.	-22.	999.	
71.23	7.	13.	17.	21.	22.	19.	24.	31.	-33.	-37.	-35.	-22.	999.	
71.38	7.	11.	17.	21.	24.	18.	19.	18.	-28.	-34.	-33.	-20.	999.	
71.53	6.	10.	19.	21.	22.	18.	19.	9.	-30.	-32.	-30.	-16.	999.	
71.68	5.	7.	19.	21.	21.	19.	19.	10.	-21.	-29.	-23.	-16.	999.	
71.83	5.	7.	18.	20.	19.	18.	14.	7.	-24.	-28.	-23.	-14.	-10.	
71.98	4.	6.	17.	19.	18.	15.	10.	5.	-25.	-28.	-25.	-12.	-12.	
72.13	4.	5.	13.	18.	16.	14.	9.	3.	-24.	-26.	-22.	-7.	-12.	
72.28	4.	5.	7.	17.	15.	13.	5.	1.	-21.	-22.	-21.	-7.	-12.	
72.43	3.	4.	4.	15.	15.	11.	6.	0.	-21.	-21.	-18.	-10.	-11.	
72.58	2.	3.	4.	13.	14.	9.	4.	-1.	-17.	-21.	-16.	-9.	-10.	
72.73	1.	3.	4.	9.	11.	7.	3.	-2.	-20.	-18.	-14.	-10.	-10.	
72.88	1.	1.	2.	7.	9.	6.	3.	-4.	-16.	-18.	-12.	-10.	-10.	
73.03	1.	0.	0.	1.	7.	5.	0.	-6.	-12.	-18.	-14.	-9.	-11.	
73.18	0.	0.	-1.	0.	2.	2.	-2.	-6.	-13.	-15.	-15.	-10.	-9.	
73.33	0.	-1.	-2.	-2.	-1.	2.	-3.	-13.	-11.	-15.	-13.	-7.	-6.	
73.48	-1.	-2.	-3.	-4.	-3.	0.	-6.	-13.	-11.	-13.	-11.	-7.	-7.	

Figure 7: Mean Doppler velocities in an azimuth range format with the outline of the mesocyclonic shear feature.

contour; it must have a diameter of at least 10 km and an identifiable core. So the two probabilities for a scan (defined by azimuthal limits of the antenna or 360° if rotation is continuous) are:

$$P_{fa} = N_f/N_c;\ P_d = N_d/N_{cd} \tag{20}$$

where N_f is the number of false alarms, N_d the number of detections, N_{cd} the true number of mesocyclonic shears (M) in a scan and N_c the number of cells if there is not more than one false alarm per cell. With more than one false alarm per cell, the number of cells should be increased by the number of multiple false alarms in order to ensure that none of the probabilities ever exceeds one.

Even though we had three or four cases where there were multiple false alarms, we chose not to increase the number of cells because we never had more false alarms than cells (i.e., if there were 3 cells and one of them had 2 false alarms, we assigned a 2/3 probability of false alarm per cell for that scan). Similarly, if a cell had both detection and false alarm we counted such a false alarm inspite of the fact that in an operation situation such a false alarm would not count. The algorithm is tested only at heights lower than 8 km because at high altitudes divergent flow dominates, and a divergence-measuring algorithm should be utilized there. Furthermore, we do not examine data beyond 230 km, which is the stipulated maximum range where Doppler measurements are required from the NEXRAD.

The algorithm was tested on data from several tornadic days (see Table 2 for a description of severe weather), and the results follow:

April 5, 1978: On this day data were collected in a continuous 360° scan mode as part of a Joint Doppler Operational Project (JDOP) experiment (JDOP staff, 1979). Three volume scans were analyzed, and the results for one are given in Table 3. The storms on this day developed in a broken line (Figs. 8a, b), and there were anywhere from 10 (at low elevations) to 6 cells (at higher elevations) per PPI. The southern storm developed circulation first. The false alarms occurred mainly in that storm because it was located in the second trip area where first-trip ground clutter contaminated measurements.

TABLE 2

Severe Weather List

Date	Time	Location	Mesocyclone Associated	Damage Description
5 April 1978	1910-1920	Center of line	Yes	Wind damage
	1930	SW end of line	Yes	Wind and hail damage
	1955-2005	SW end of line	Yes	Tornado-caused extensive damage along a 20-km path
30 April 1978	1820-1835	Cell near radar	Yes	Tornado-caused severe damage along a 14-km path
2 May 1979	1600	Eastern cell	Yes	Severe hail damage
	1610-1715	Eastern cell	Yes	Tornado-caused severe damage along a 50-km path
	1617-1705	Center cell	Yes	Tornado-caused moderate damage along a 45-km path
	1635	Eastern cell	Yes	Large hail reported
	1700	Center cell	Yes	Large hail reported
22 May 1981	1849-1926	Eastern cell	Yes	Tornado-caused very severe damage along a 30-km path near Binger, OK
	1900	Center cell	Yes	Tornado-caused light damage along a several km path
	1932-1935	Eastern cell	Yes	Tornado-caused light damage along a 5-km path
	1955-2010	Western cell	Yes	Tornado-caused moderate damage along a 15-km path

*All reported severe weather during the four time periods of algorithm testing is given in this table. Note that all severe weather was associated with detected mesocyclones.

TABLE 3

Results for Volume Scan at 1855 CST, April 5, 1978

El.	No. of Cells	No. of Detected M	No. of Detections in Ground Clutter	True Number of Mesoshears	P^*_{fa}	P_{fa}	P_d
1	10	5	2	1	.4	.2	1
2	9	3	2	0	.33	.22	
3	7	3	1	0	.42	.14	
4	6	1	0	0	.16	.16	
5	6	0	0	0	0	0	

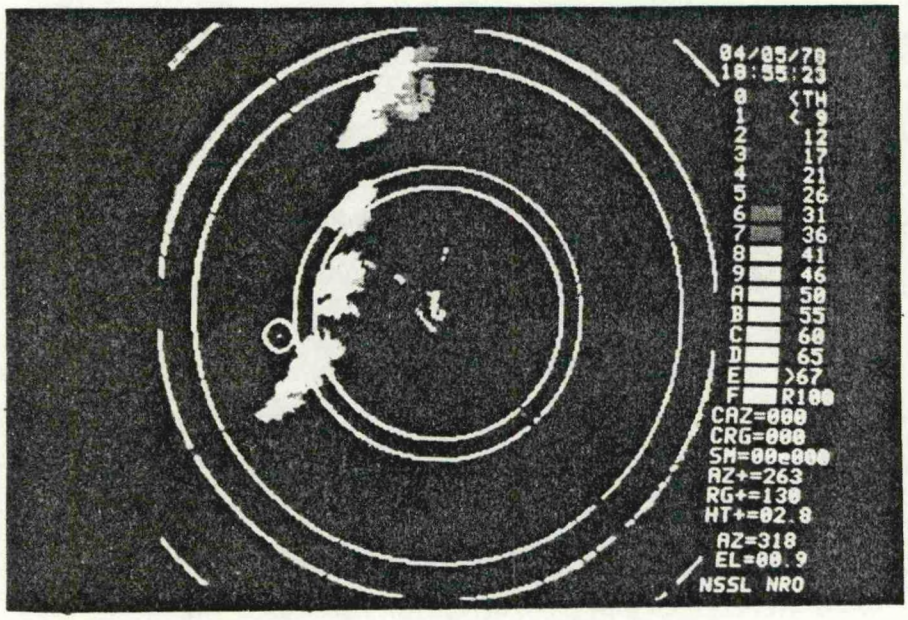

Figure 8a: Reflectivity display of the storm complex on April 5, 1978, at 1855 CST. Range rings are at 100 km, 115 km, 200 km and 230 km.

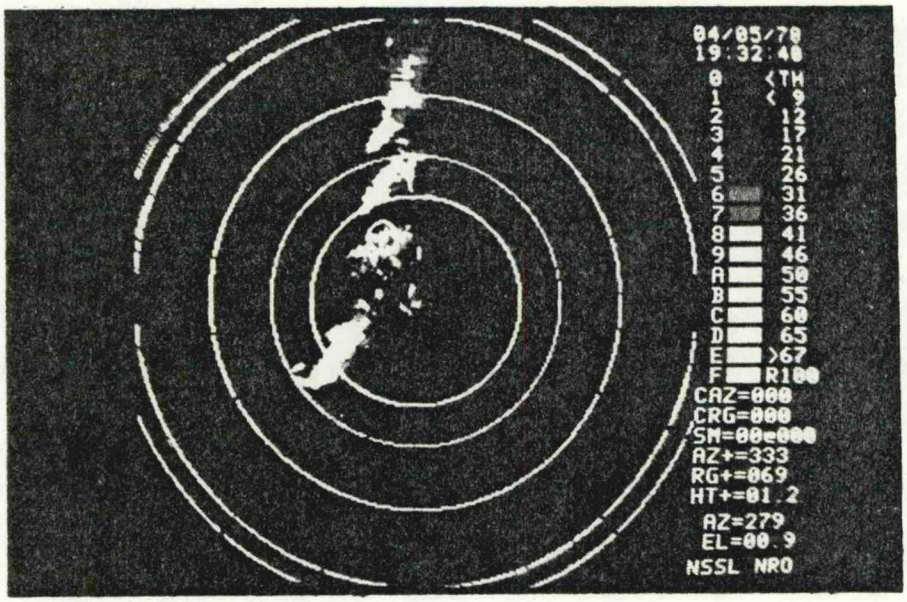

Figure 8b: Same as (a) but at 1932 CST. Range rings are at 100 km, 138 km, 200 km, 276 km and 300 km.

For example, in Fig. 9a the multimoment display (Burgess et al., 1976) at 0.9° has a large number of inconsistent arrows and arrows with large arrowheads corresponding to increased spectrum width due to ground clutter. The algorithm classified as mesocyclonic shear the data with centers at r = 140 km, az = 238°; r = 143 km, az = 241°; r = 135 km, az = 242.8°; and r = 162 km, az = 238.5°. The last center corresponds to the only one genuine mesocyclonic shear; the rest of the centers are associated with the ground clutter contaminated data. Even though only data with signal strengths at least 10 dB above clutter are retained, the clutter spectrum is much narrower than the signal spectrum so that coherent processing enhances the clutter that much more. The 10-dB criterion ensures that errors are below 1 $m \cdot s^{-1}$ only if the signal spectrum width does not exceed the one from clutter (Hennington, 1981). Dots on Fig. 9 indicate data where the criterion is not met. Note that the spectral moments displayed on this figure are spaced 2.55 km apart. To give the reader a better appreciation of the contamination, we present on Fig. 9b a portion of this data field where the moments are spaced every 300 m in range. The obviously incoherent nature of the velocities and large spectrum widths are the consequence of ground clutter interference. Therefore, we decided to discriminate between bad data and good data (in this case only). So the probability of false alarm P^*_{fa} is for all data whereas P_{fa} is for good data only. Later, the storm moved out of the clutter area, and the performance improved. We summarize the results in Table 4.

It is satisfying that the probability of detection is 1, since the algorithm was designed to be conservative and not miss any potentially hazardous feature. This is the reason for the false alarm probability of about 0.1. This number would be reduced if vertical continuity were utilized. To be on the conservative side, let us assume that if one out of three consecutive shears in height is classified as mesocyclonic, the whole event will be declared a mesocyclone. Then for our data there would have been one false alarm (in the first of three volume scans). Two of the false alarms resulted from incorrect dealiasing of radial velocities.

For this and all other analyses, storm motion was removed from the mean radial velocities. Prior to the removal of storm motion, we had an increased probability of false alarm by about 20%, and worse yet, we missed detecting one true mesocyclonic shear.

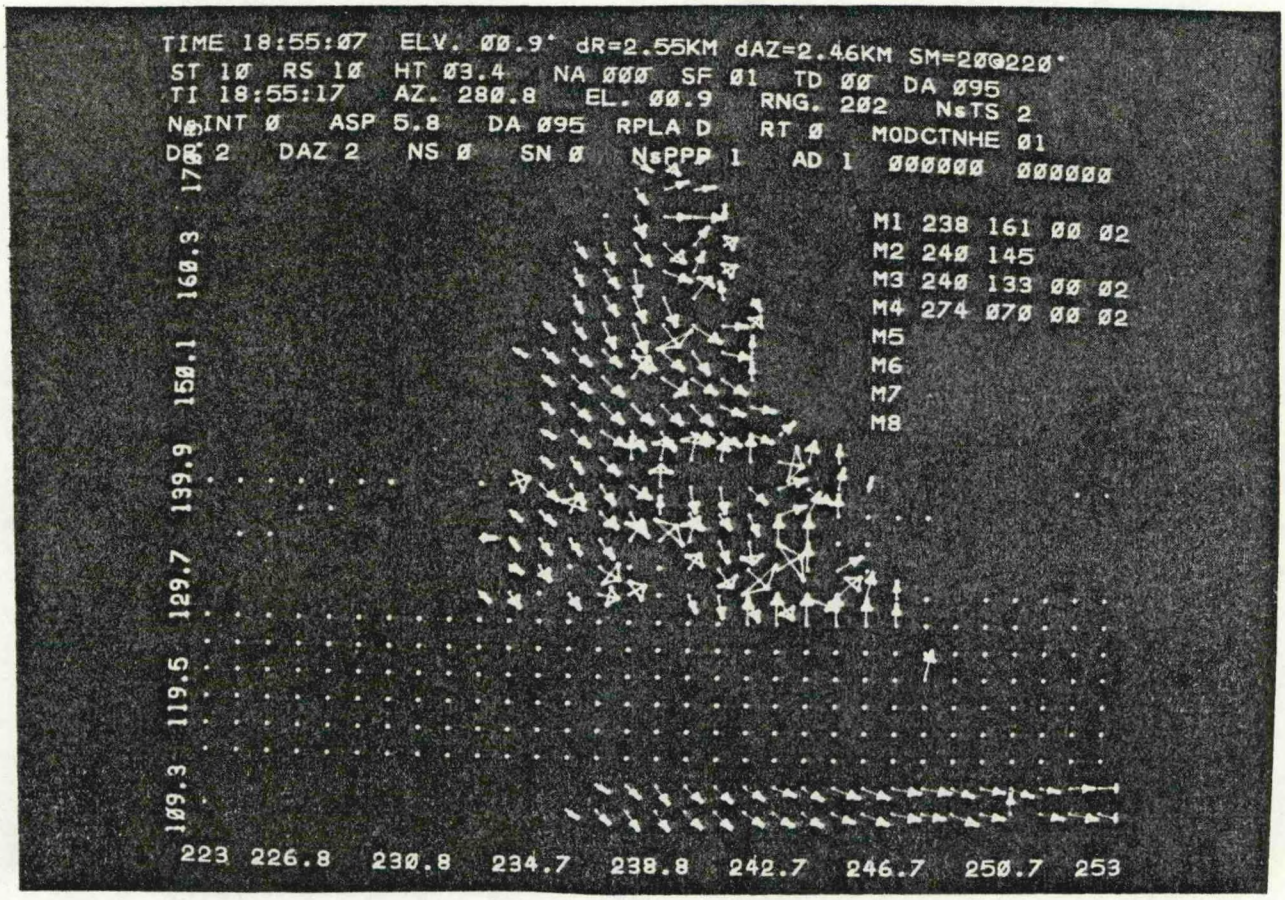

Figure 9a: Multimoment display of the southernmost cell from Fig. 8a. Arrow length is proportional to reflectivity, arrow direction to velocity (with positive between 0 and 180°) and arrowhead size to spectrum width. Azimuths are on the abscissa and ranges are on the ordinate. The first-decade digits are aligned with actual coordinates on the display. Separation between ranges is 2.55 km; elevation is 0.9°; and a storm motion of 20 $m \cdot s^{-1}$ from 220° was subtracted.

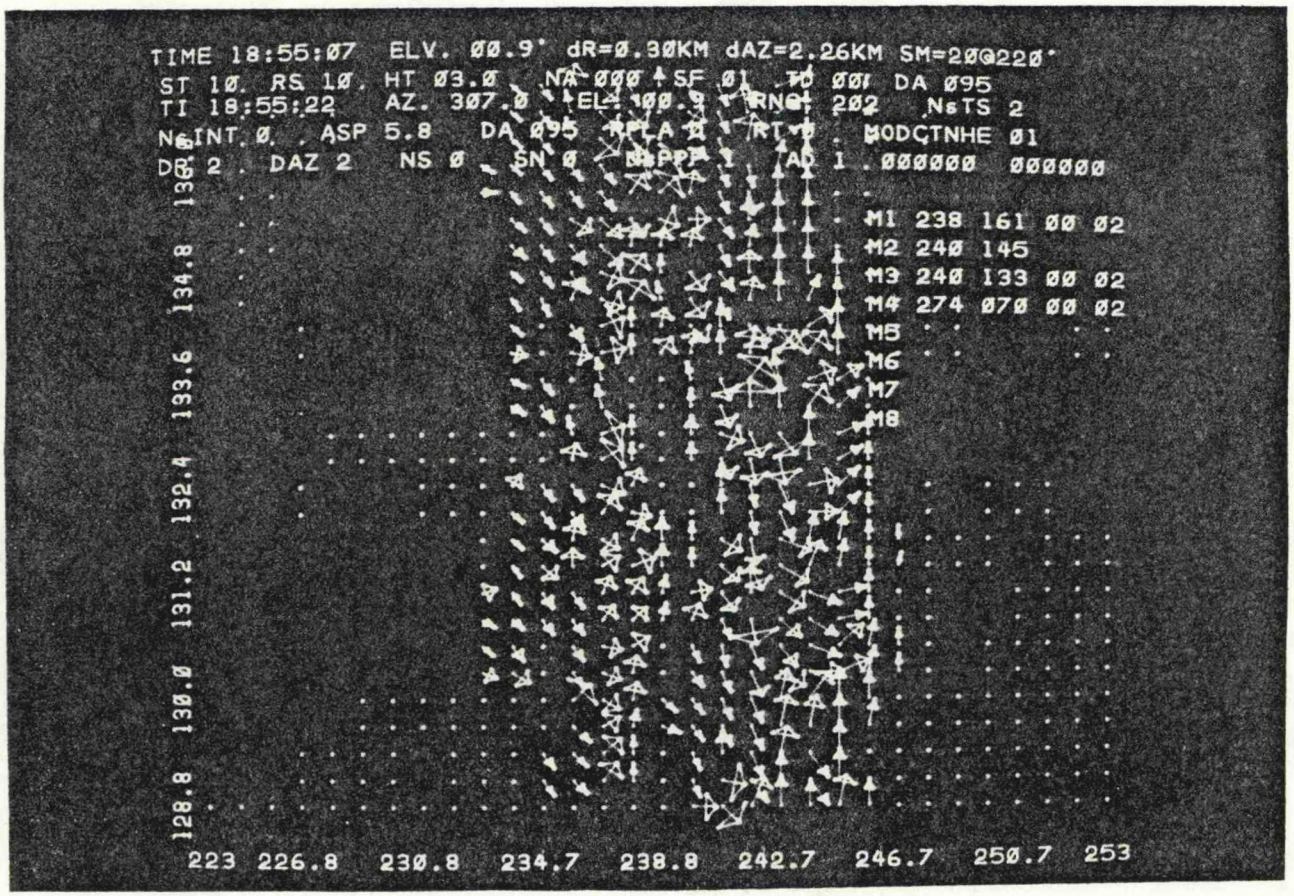

Figure 9b: Same as (a) except data separated by 300 m in range are displayed.

TABLE 4

P_{fa} and P_d for April 5, 1978, with the number of scans = 17

Beg. Time of Volume Scan	No. of Cells	No. of Detected Mesoshears	No. of Detected in Bad Data	True No. of Mesoshears	P^*_{fa} (total)	P_{fa} (in good data)	P_d
1855	38	12	5	1	0.29	0.16	1
1912	48	8	1	6	0.04	0.02	1
1944	59	21	2	13	0.13	0.1	1
			Probabilities for the 3 Volumes		0.15	0.09	1

May 22, 1981: About 2 hours of data collected from 1900 to 2100 CST were run through the algorithm. Three intense cells occurred, each of which at one time or another produced a mesocyclone (Fig. 10). The closest cell produced several mesocyclones over the period of observations. An example of tabulated values for a volume scan starting at 1915 CST demonstrates perfect detection and small probability of false alarm (Table 5). The sizes and locations for some of the features detected in the table are depicted on Figs. 11a-c. On Fig. 11b, the closer-in feature was correctly classified as shear S, but on the next height (Fig. 11c), the feature is classified as mesocyclonic shear M. This is a questionable false alarm since it passes the criterion, and furthermore, the dominant circulation is only a few kilometers away.

A summary of the P_{fa} and P_d for these volume scans is presented in Table 6a. Note, there is often a perfect detection except between the times of 1930 and 2000, when two mesocyclones were not detected (even as a shear feature)! One (r = 180 km, az = 298°) was missed at the lowest elevation of 0.3° but correctly detected at 0.9°. After lowering the reflectivity threshold to 3 dBZ, the mesocyclone at 0.3° was classified as S because of its elongated shape in azimuth (i.e., D_{az}/D_r = 2.5>2). The mesocyclone at 0.9° was misclassified as S because the sum of velocities criterion was exceeded.

Part of the same general circulation was not detected at 3° because its center had a reflectivity of 5 dBZ, which was below the threshold of 15 dBZ. This is illustrated on the multimoment display (Fig. 12a) where the "bounded weak echo region" below 15 dBZ is surrounded by arrows. Upon lowering the reflectivity threshold to 3 dBZ, the display clearly shows a circulation (Fig. 12b), which, with that threshold, was also detected and correctly classified by the algorithm.

But lowering the threshold has not helped in classification of mesocyclones in weak echo regions in subsequent scans. As a matter of fact, several times a wrong classification resulted for cases where at 15 dBZ the classification was correct. Three times the imbalance of velocities increased (for the mesocyclone at 108 km the increase was from 17.2 to 18.6 $m \cdot s^{-1}$, and for others it was over 20 $m \cdot s^{-1}$). On two occasions (at 50 km) the detection in weak reflectivities resulted in a radially elongated feature (D_r = 13.8 km, D_{az} = 0.6 km). These findings are summarized in Table 6b. Note an overall increase in P_{fa}, a decrease of P_d for three volume scans and an improvement in

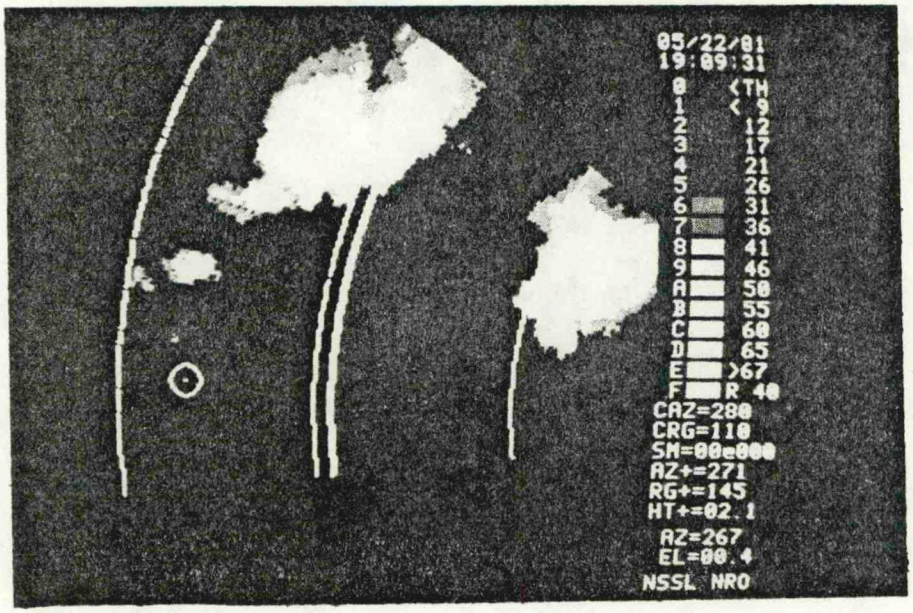

Figure 10: Reflectivity display at 1909 on May 22, 1981. Range marks are 40 km apart, with the first one at 80 km. Interference ring is at 115 km.

TABLE 5

Results For A Volume Scan at 1915 CST, May 22, 1981

El.	No. of Cells	No. of Detected Features	No. Classified as Mesoshears	No. of Recognized Mesoshears	No. of Mesoshears Classified as Shear	No. of Mesoshears Not Identified as Features	True Number of Mesoshears	P_d	P_{fa}
0.4	3	1	1	1	0	0	1	1	0
0.8	3	1	1	1	0	0	1	1	0
1.2	3	2	2	1	0	0	1	1	0.33
2.4	3	3	1	1	0	0	1	1	0
3.4	3	3	1	1	0	0	1	1	0
4.4	1	4	2	1	0	0	1	1	1
5.4	1	1	1	1	0	0	1	1	0
6.5	1	2	2	1	0	0	1	1	0

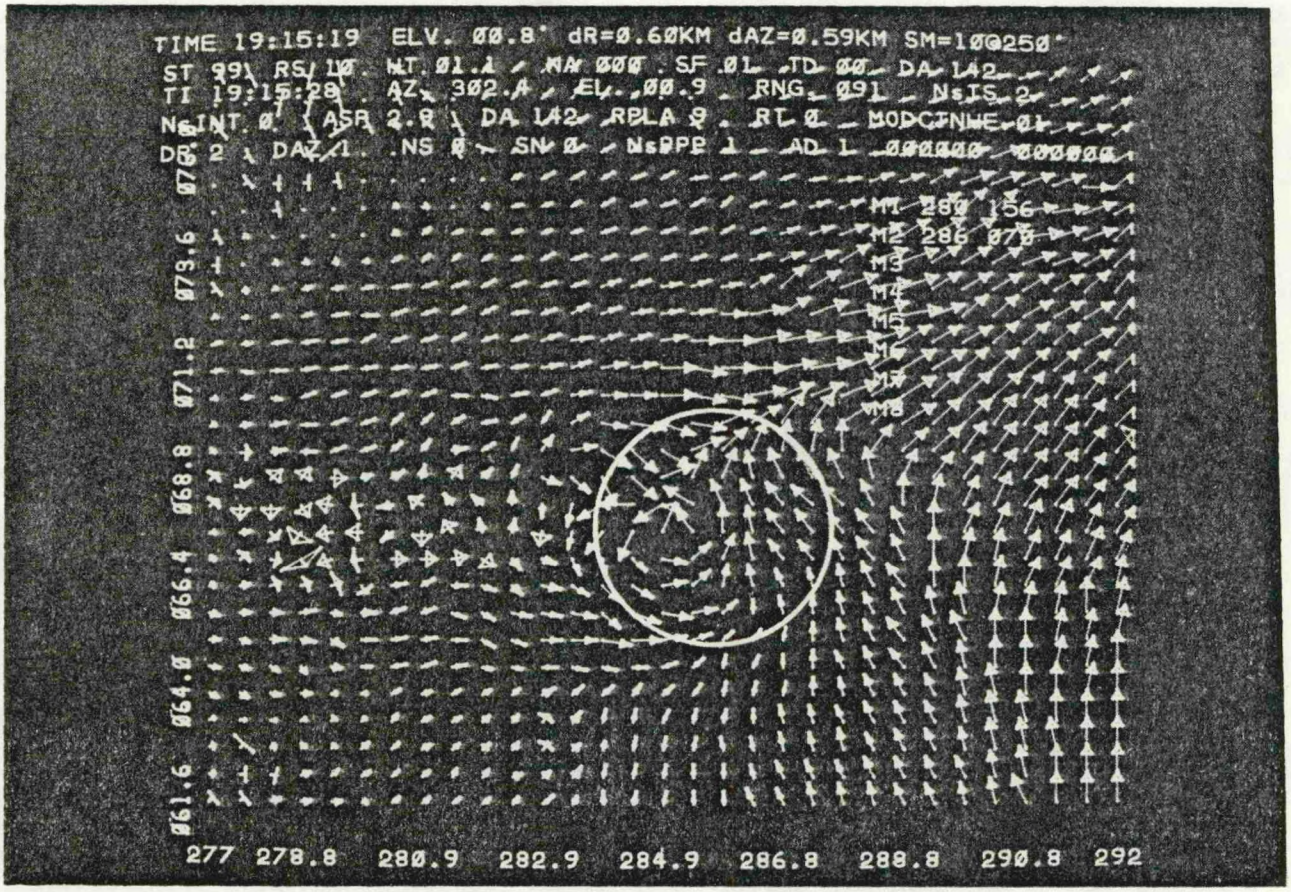

Figure 11a: Multimoment display of a portion of the cell at 65 km from the radar (Fig. 10). Data are spaced in range at 0.6 km. The mesocyclonic shear is encompassed by a circle whose diameter equals the estimated diameter from the algorithm. In this example, both range and azimuth diameters were equal. Storm motion of 12 m·s^{-1} from 250° has been removed; elevation angle is 0.8°.

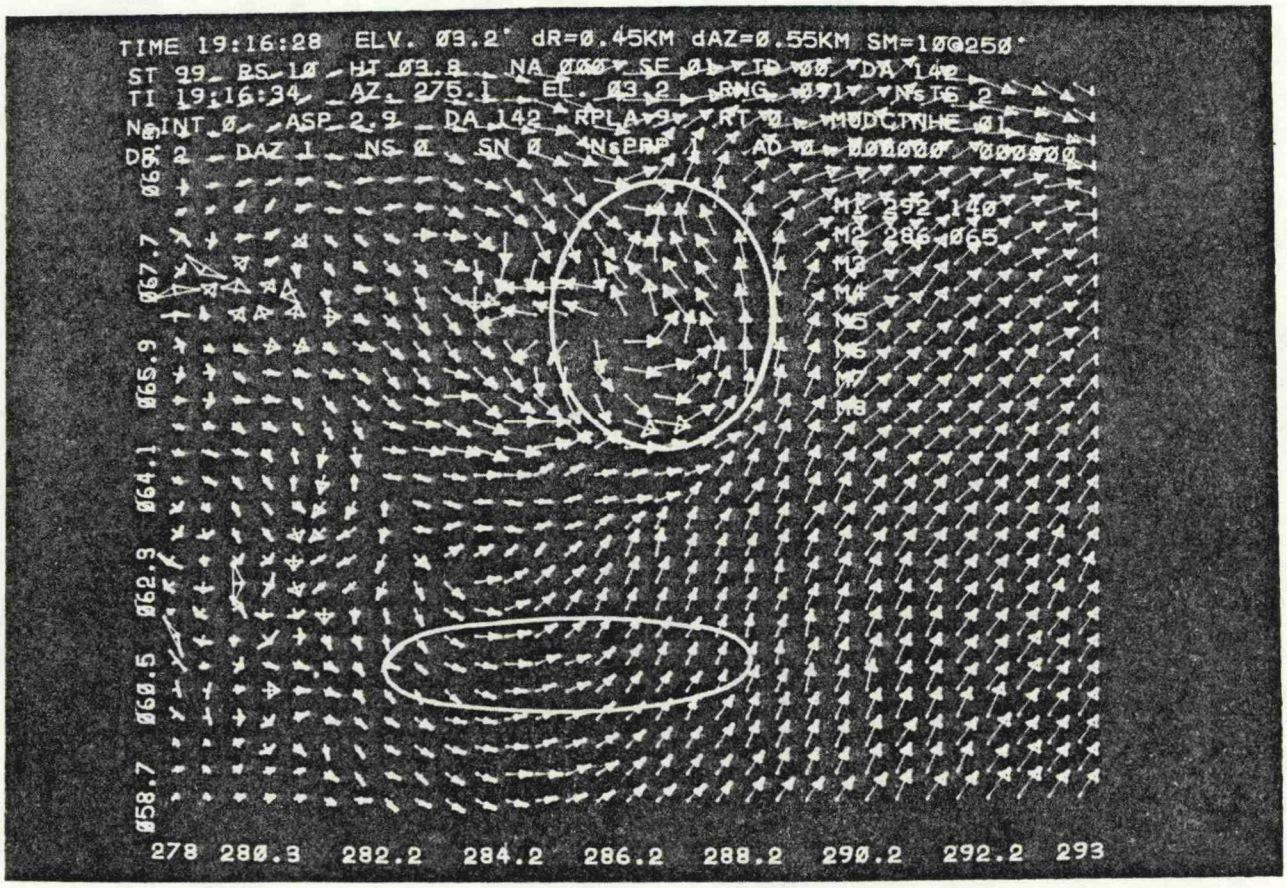

Figure 11b: Multimoment display at 3.2° in elevation. The closer-in feature was identified as shear, and the ellipse was drawn from the estimated azimuthal and range dimensions. The further-out feature was correctly identified as mesocyclonic shear. Data are spaced at 0.45 km in range.

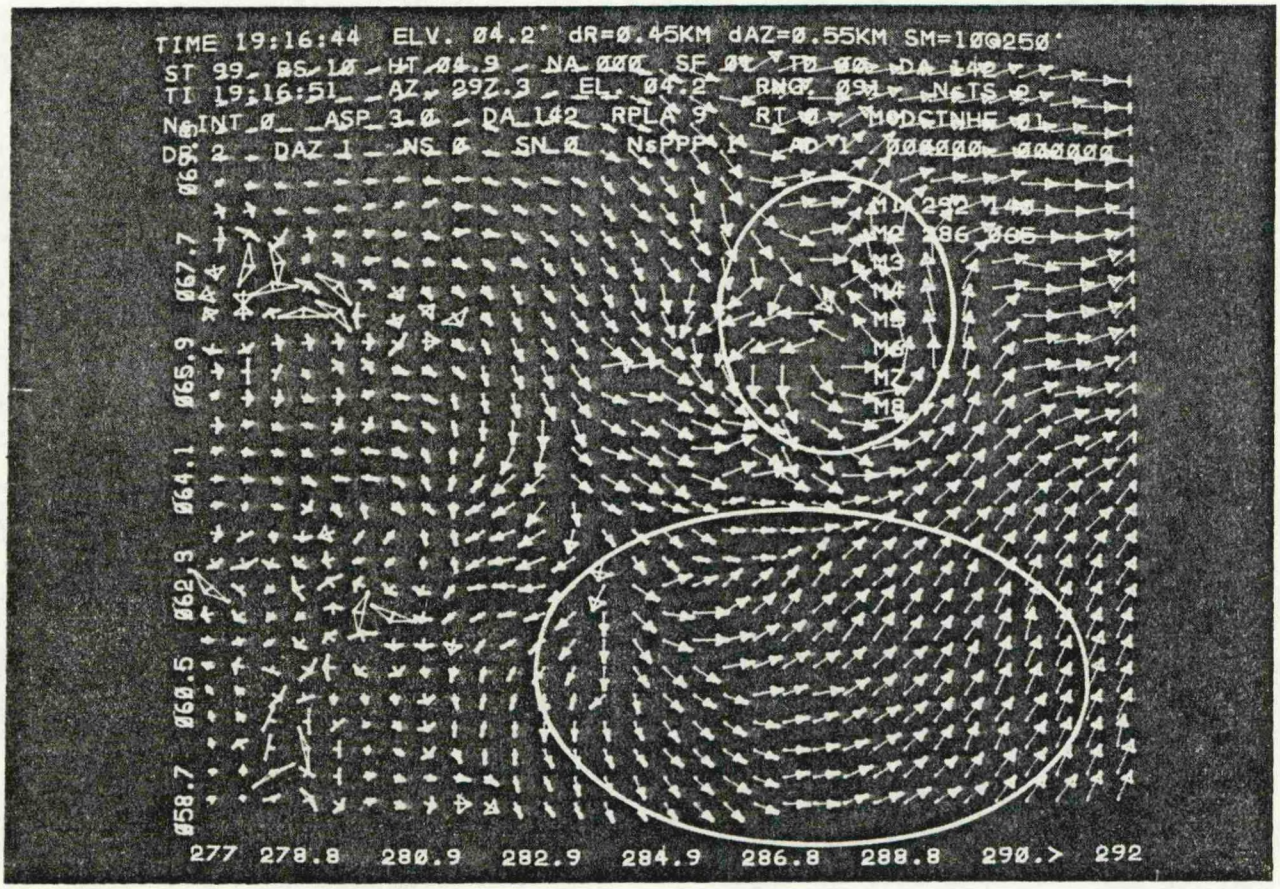

Figure 11c: Same as (b) but at 4.2° in elevation. Both features were classified as mesocyclonic shears.

TABLE 6a

P_{fa} and P_d for May 22, 1981

Beg. Time of Volume Scan	No. of Cells	No. Classified as Mesoshear	True No.	P_{fa}	P_d
1909	18	10	9	0.1	1
1915	18	11	8	0.05	1
1929	27	8	7	0.04	1
1931	19	13	14	0	0.92
1937	19	7	6	0.05	1
1942	19	5	5	0.05	0.8
1946	20	4	4	0.05	0.5
1952	20	6	5	0.15	0.6
1957	20	4	2	0.15	0.5
2000	20	8	5	0.25	0.6
2008	24	5	3	0.08	1
2014	12	4	2	0.16	1
2018	12	5	1	0.3	1
2027	12	5	4	0.08	1
2032	14	6	2	0.28	1
2038	14	2	1	0.07	1
2043	13	3	2	0.08	1
2049	13	6	2	0.3	1
		Total for the Day		0.09	0.89

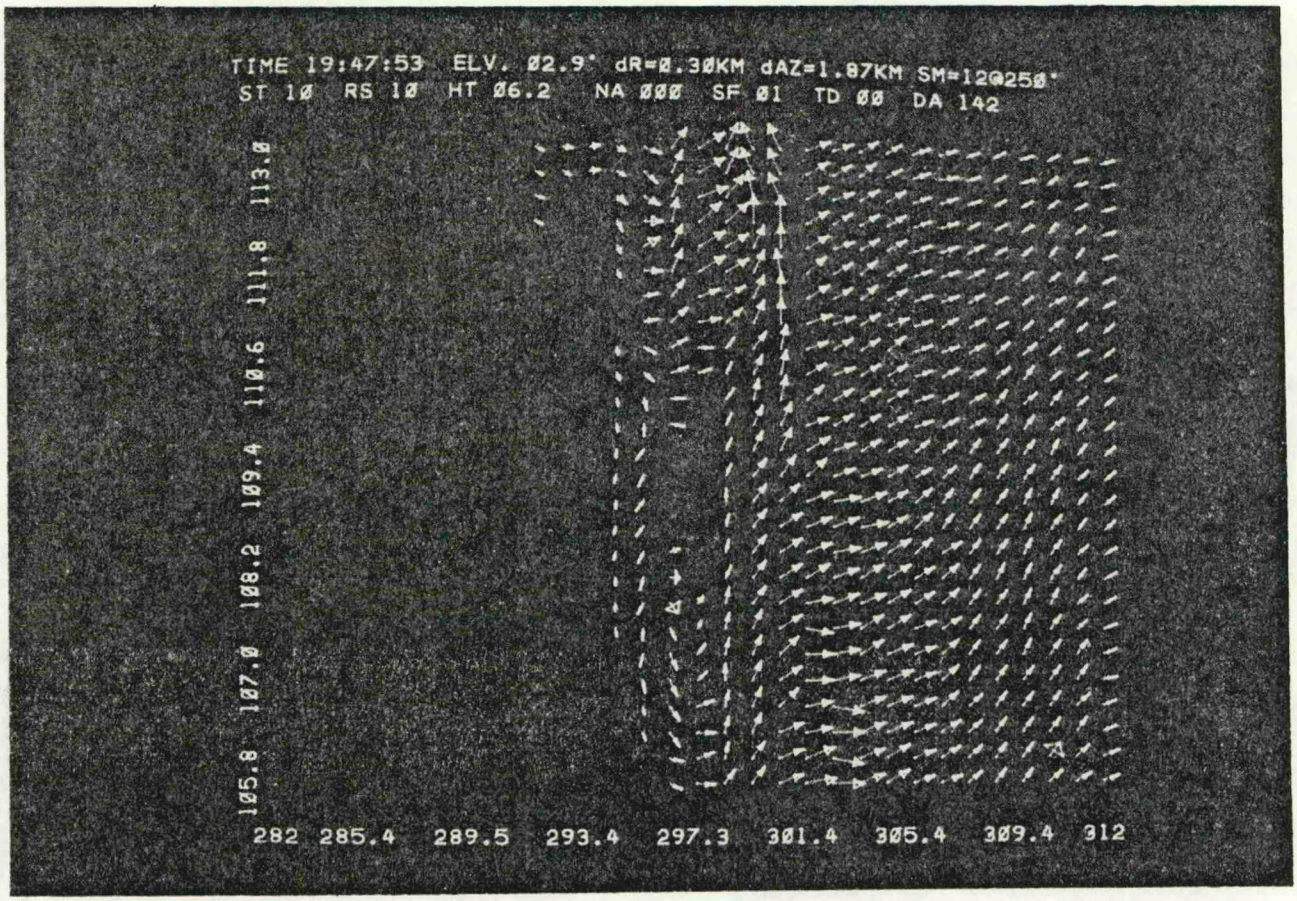

Figure 12a: Multimoment display of a cell at 100 km on May 22, 1981, at 1947 CST. Elevation is 2.9° and data are spaced 0.3 km in range. The lack of data in the middle of circulation is due to low reflectivities (about 5 dBZ), which are below the display threshold of 15 dBZ.

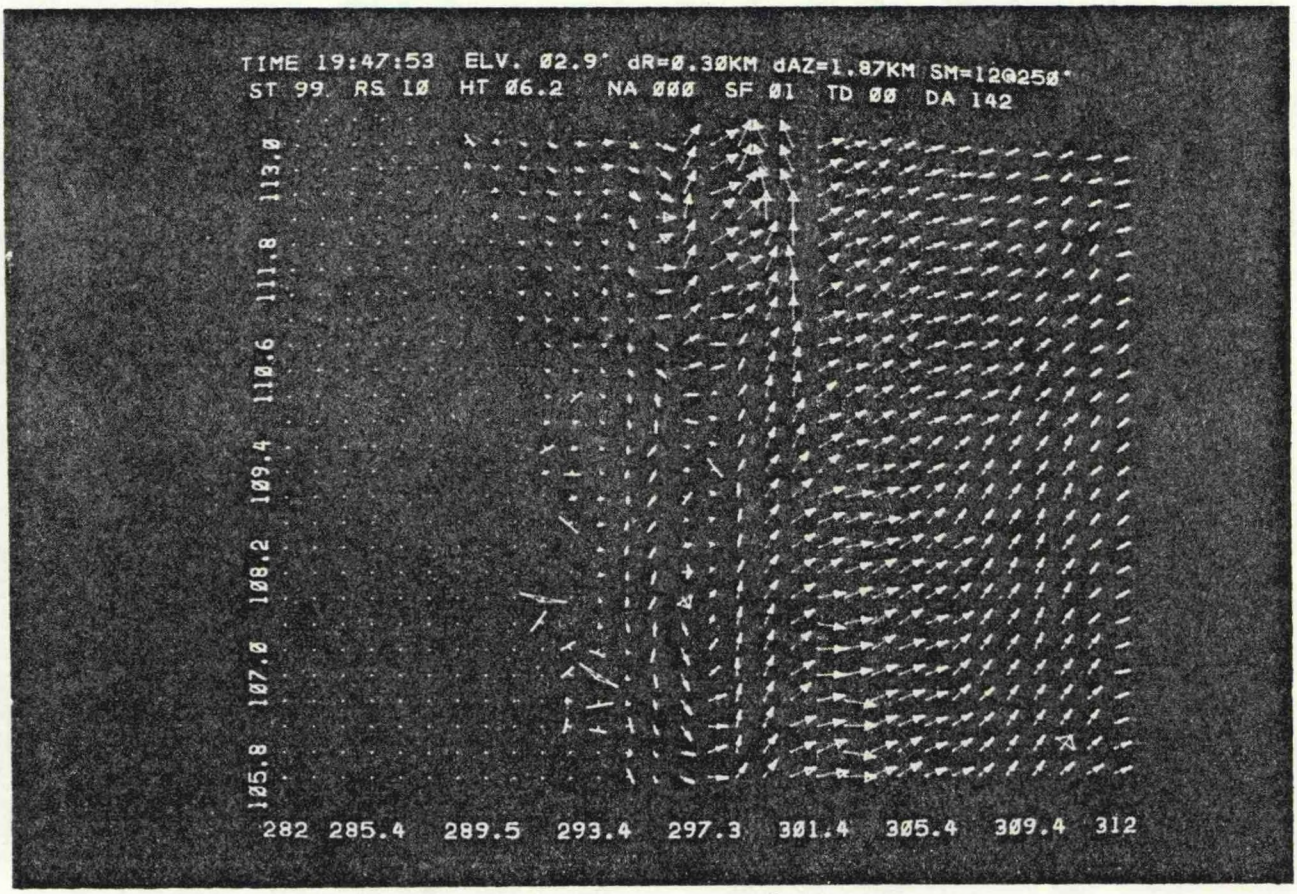

Figure 12b: Same as (a) except the reflectivity threshold for display of data has been eliminated. The circulation is clearly visible and its apparent asymmetry is due to unequal scales on the axes.

TABLE 6b

P_{fa} and P_d for 22 May 1981 with RTH=3 dB

Beginning Time of Volume Scan	P_{fa}	P_d
1929	0.18	1
1931	0.02	0.92
1937	0.05	0.5
1942	0.1	0.66
1946	0.2	1
1952	0.3	0.4
1957	0.45	0.5
2000	0.7	0.6

P_d in only one scan! It therefore seems prudent to stay with a reflectivity threshold of about 15 dBZ, but exhaustive tests are needed to determine the optimum value.

Next we show some characteristic parameters of mesocyclonic shear as estimated by the algorithm. On Figs. 13a,b are the azimuthal radii and the range radii versus height for two consecutive volume scans. Note that there is a good consistency of values both in height and in time. The feature above 8 km on Fig. 13a was classified as shear since $D_r > 2D_i$ (i = 1, 2, 3). At this height divergence becomes significant, and we do not recommend use of the algorithm above 8 km. At about 3 km, the algorithm began to discriminate between two circulations. We plotted the parameters for the stronger one (see Fig. 11b); however, at 6 km the algorithm merged both circulations to one, and therefore $D_r/2$ increased at that height (on Fig. 13a and b). Because the mesocyclone is large and angular resolution good, the four diameters should be related by $D_r > D_2 > D_1 > D_3$. This relationship is valid for 13 out of 18 cases plotted on Figs. 13a, b.

The average momentum, shear and rotational speed estimated by the algorithm for the same volume scans are plotted on Figs. 13c, d. The consistency of these quantities is good, with the rotational speed and the shear slightly decreasing with height as observed by Burgess et al. (1982) for mesocyclones in the mature stage of development.

Another example on Fig. 14 demonstrates the evolution of mesocyclone parameters, from first detection to final dissipation, as a function of time. Note that $D_r < D_3 < D_1 < D_2$ and furthermore $D_r < 2D_1$ at about 1930 CST. Azimuthal smoothing at long ranges (150 km) causes this asymmetry, and it has forced us to amend our classification criterion. When first detected (1915 CST), only one feature was present, but in subsequent scans two rotations with centers spaced about 2 to 5 km apart were detected and confirmed. We plotted data for one of these which was persistent and in "steady-state" up to 1925 CST. After that time a more pronounced change occurred: the center of the mesocyclone shifted (2 km and 3°) and had a more erratic movement from then on. We attribute this to the turbulent dissipation of the vortex. Indeed at 1947 CST the circulation was classified as shear (but was present at three consecutive heights). Five minutes later shear was present only at two heights; after another five minutes, S was present at

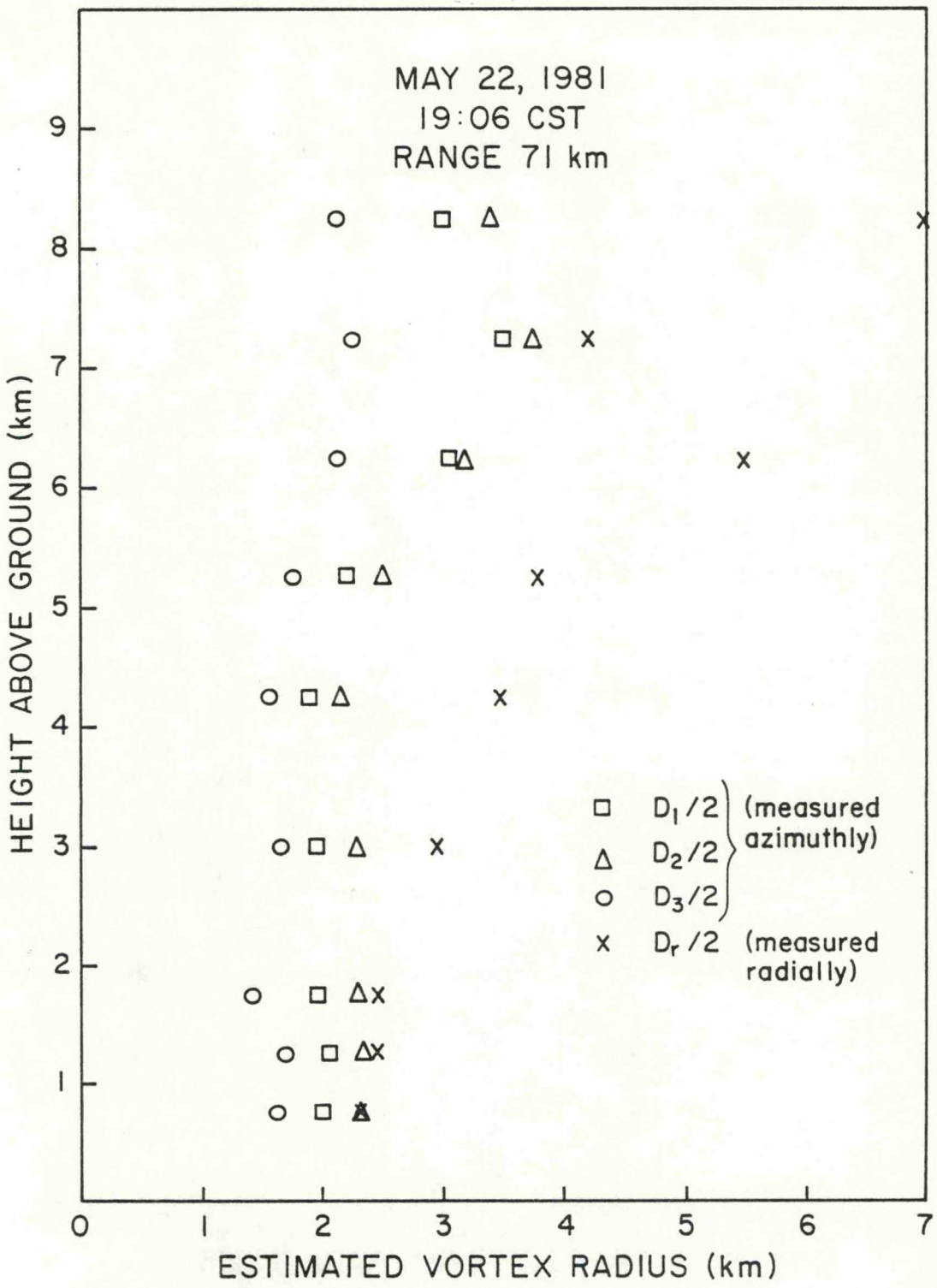

Figure 13a: Estimated radii versus height for a mesocyclone 70 km from the radar, at 1906 CST.

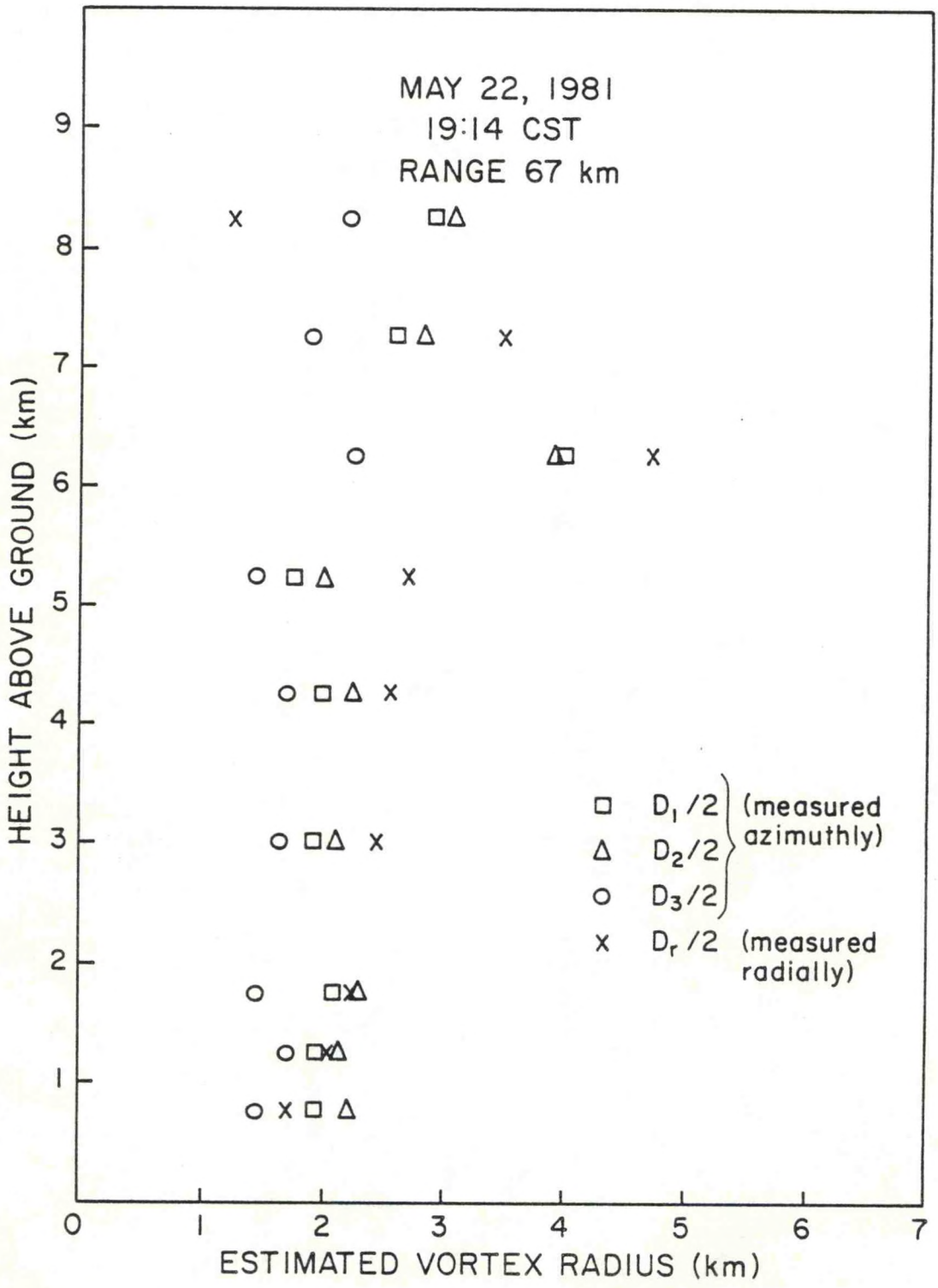

Figure 13b: Same as (a) except at 1914 CST.

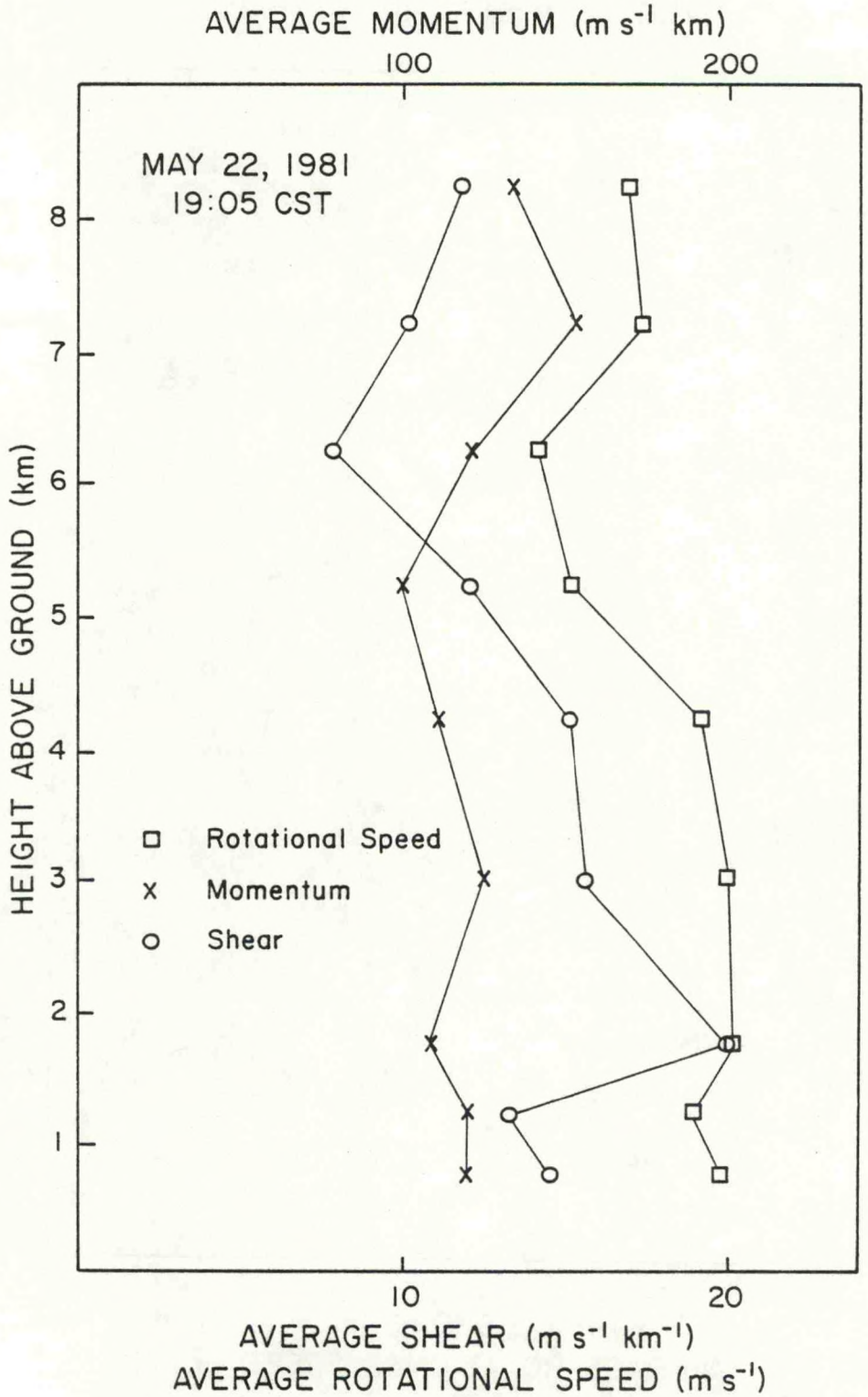

Figure 13c: Estimates of average shear, momentum and rotational speed at 1906 CST.

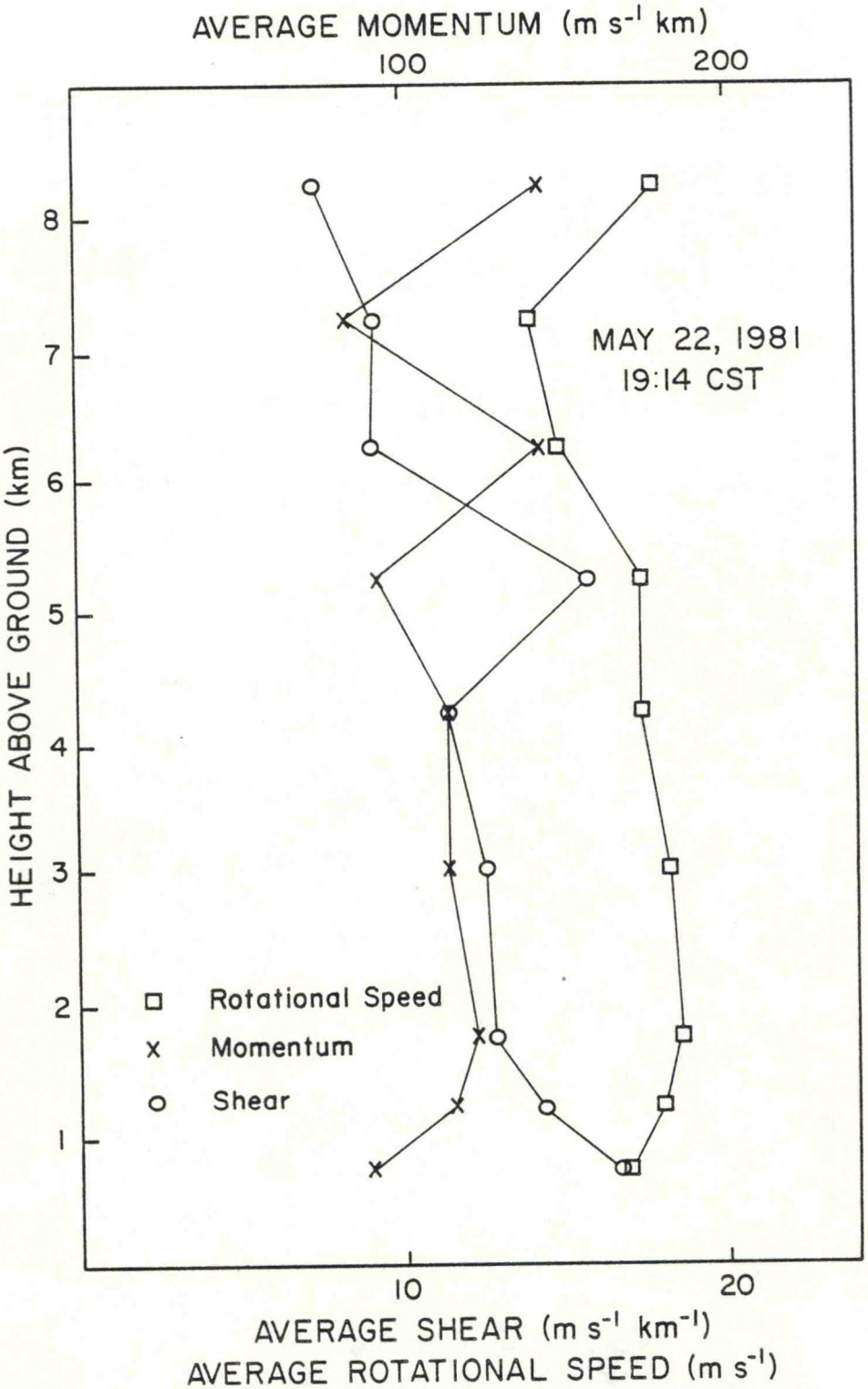

Figure 13d: Same as (c) but at 1914 CST.

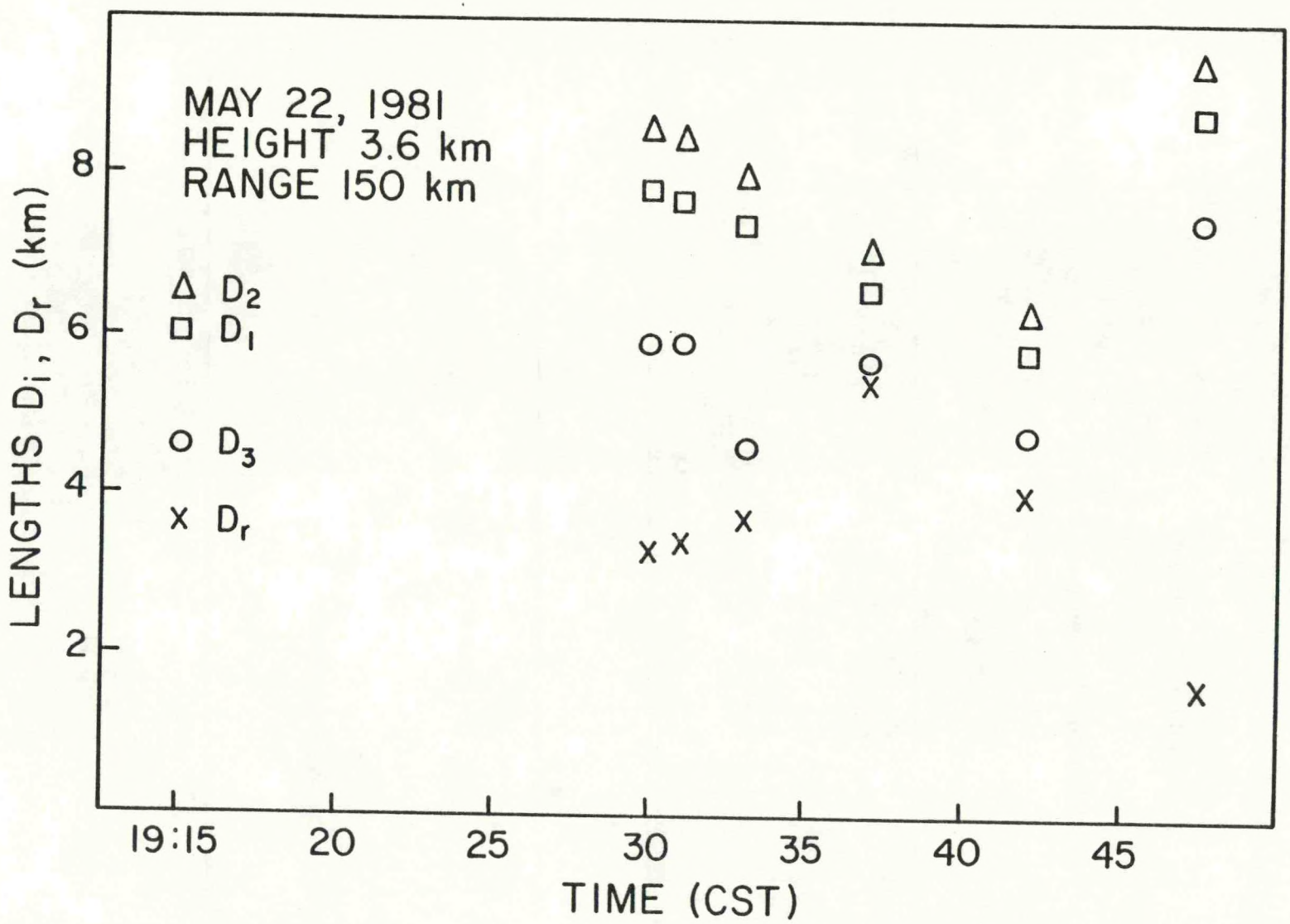

Figure 14a: Azimuthal and range "diameters" estimated by the algorithm versus time at a constant height. The mesocyclone was at 150 km from the radar. Data points start at 1915.

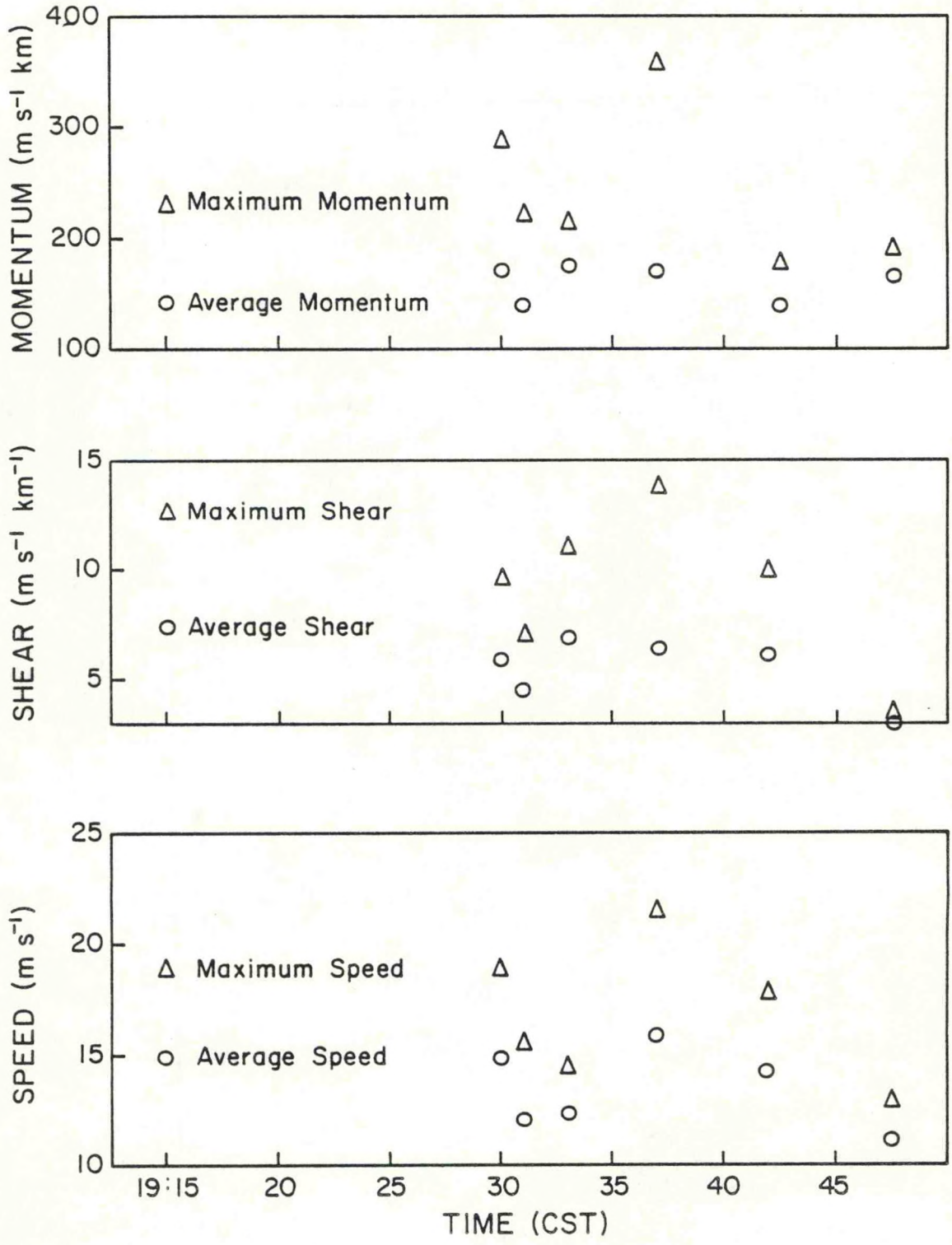

Figure 14b,c,d: *(b) Momentum for the same data as on (a).*
(c) Shear for the data on (a).
(d) Rotational speed for the data on (a).

another two heights; and subsequently no feature was detected in that cell by either man or the algorithm.

April 30, 1978: Two volume scans over a period of 10 minutes were subjected to the algorithm; Table 7 gives the succinct results. Display of velocities on Fig. 15a illustrates the storm distribution on this day. The cell at 50 km in range and 340° in azimuth produced a severe tornado and the cell at 220 km and 310° had a mesocyclonic shear in the lowest level (0.2°). The expanded version on Fig. 15b of the closer (Piedmont) storm contains a clearly defined circulation pattern. The center of this pattern coincides with the center calculated by the algorithm (cursor position on Fig. 15b).

We note that the overall probability of false alarm is insignificant whereas the detection probability is 0.86. Actually two features were not properly classified. One at the height of 5 km had a large imbalance of velocities (25 $m \cdot s^{-1}$). This miss would be of no consequence because at all lower heights and in the previous scan the circulation was correctly identified. A distinct tornado vortex signature (TVS) developed at the three lowest elevation angles during the second volume scan. This signature was classified twice as an M shear and once as a shear. We have included this miss in our statistics although the centers of the mesocyclone and the TVS are less than 3 km apart. Furthermore, the algorithm has not been optimized to classify tornado vortex signatures. From available data, it seems that larger asymmetry (in the azimuthal direction) must be allowed for TVS classification. A three times larger azimuthal length than range length may be adequate. In conjunction with this criterion it may be advantageous to employ a threshold on the average rotational speed of about 15 $m \cdot s^{-1}$ and average shear of about 20 $m \cdot s^{-1} \cdot km^{-1}$. These values have been exceeded by tornado vortex signatures encountered in our data.

May 2, 1979: Three intense cells (Fig. 16) that developed on this day have been a subject of considerable investigation by scientists from the Severe Environmental Storms and Mesoscale Experiment (SESAME). One hour of data was subjected to the algorithm, and the summary is given in Table 8. There are several reasons why some of the detection probabilities are less than one. First, in nine occasions the imbalance of velocities was larger than 18 $m \cdot s^{-1}$. This occurred because the estimated storm motion did not

TABLE 7

P_{fa} and P_d for April 30, 1978

Beginning Time of Volume Scan	No. of Cells	No. of Features Classified as M	True Number of M	P_{fa}	P_d
1823	29	8	7	0.035	1
1829	27	6	8	0	0.625
			TOTALS	0.017	0.87

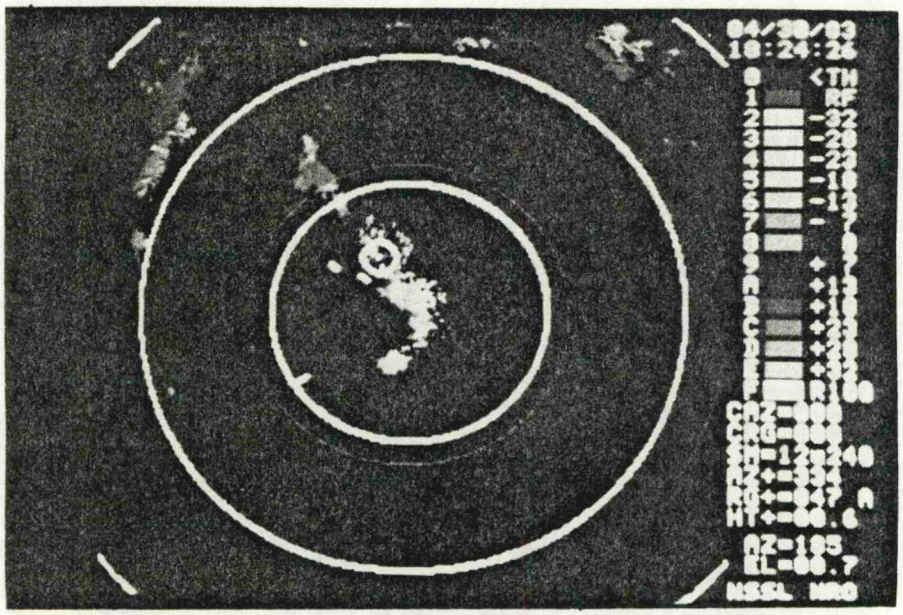

Figure 15a: Velocity display of storm cells up to 250 km in range on April 30, 1978. Range rings are 100 km apart and the cursor locates Piedmont storm.

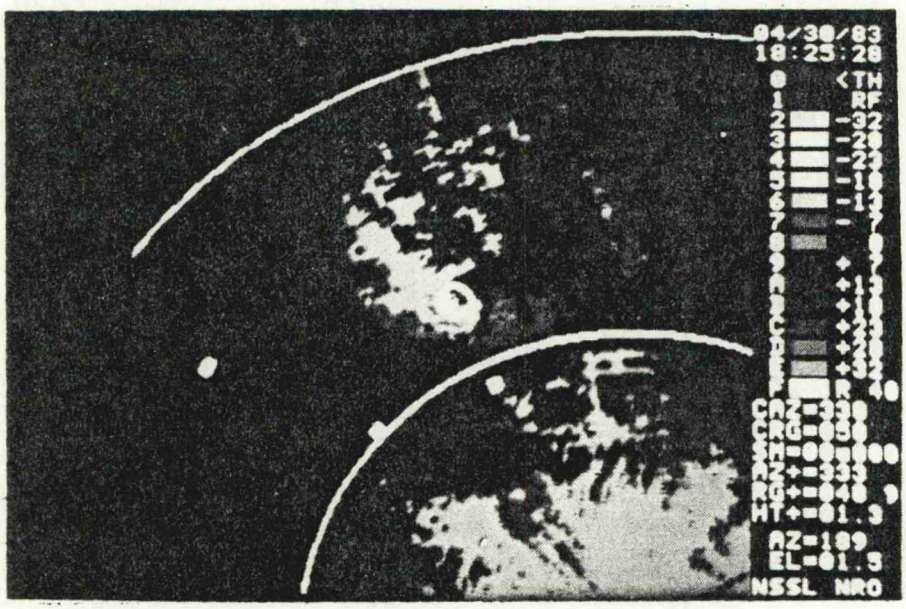

Figure 15b: Enlarged display of the Piedmont storm. Range marks are 40 km apart and the cursor is at the location of mesocyclone center as determined by the algorithm.

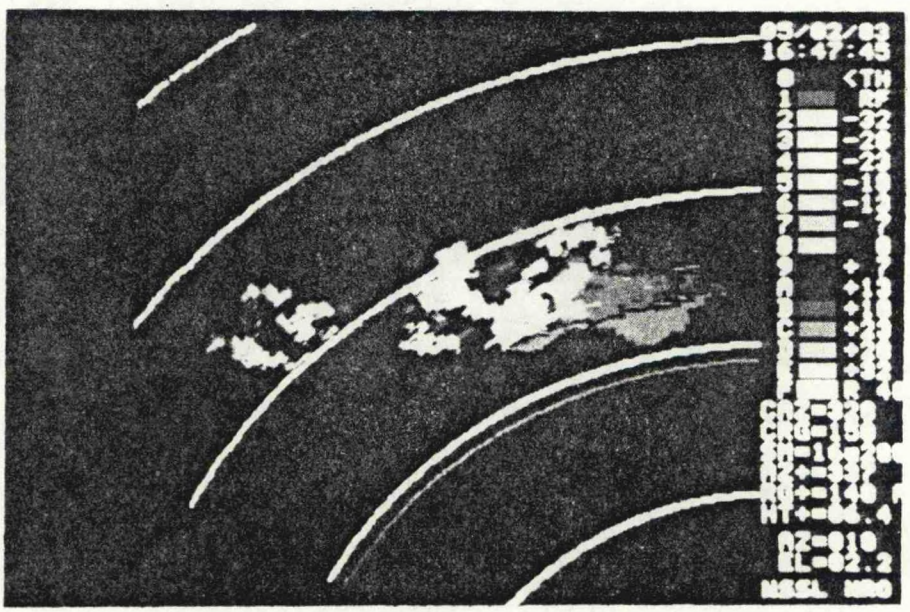

Figure 16: Velocity display of the three storm cells that occurred on May 2, 1979. Range marks are 40 km apart and start at 80 km. The cursor locates where the algorithm detected one of the three mesocyclones in these cells.

TABLE 8

P_{fa} and P_d for May 2, 1979

Beg. Time of Volume Scan	No. of Cells	No. of Features Classified as M	True No. of M	P_{fa}	P_d
1602	13	6	6	0.08	0.83
1614	17	7	4	0.18	1.0
1628	20	18	12	0.3	1.0
1638	17	6	7	0	0.86
1642	20	8	8	0.1	0.75
1646	19	12	12	0.16	0.66
1650	13	9	5	0.31	1.0
1654	17	9	8	0.06	0.88
1658	17	14	14	0.18	0.64
1702	17	11	10	0.06	1.0
1705	17	10	7	0.35	1.0
			TOTALS	0.16	0.81

correspond to the mesoscale motion: two close cells with mesocyclones were moving in an almost rotational fashion with respect to each other. Thus, with a better estimate of mesocyclone motion an improvement from 0.85 to 0.95 in P_d is achievable. But in real time it is difficult to make the estimate. Of course, we could drop altogether the balance of the velocity criterion which would result in an increase of P_{fa}. Some of the misclassifications due to imbalance of velocities included tornado vortex signatures; these could be picked up if high rotational speed and shear criteria are used. Improper velocity dealiasing and low reflectivities were the cause of some other misses.

In all the scans except at 1658 CST the radar's unambiguous velocity was 34 $m \cdot s^{-1}$. At 1658 the unambiguous velocity was only 21 $m \cdot s^{-1}$, and that is when the P_d was lowest. Out of 94 mesocyclonic shears, only 4 were not identified as features (i.e., either S or M). This was due to bad velocity dealiasing and low reflectivities.

4. Summary

Radial velocity data from 4 days were passed through a mesocyclone detection algorithm. Some 16 different mesocyclones were present in these data, and the performance against each one of these is listed in Table 9. If we average the detection probabilities for the 4 days, we obtain 0.9, but if we take the ratio of all detected to all known mesocyclones, we have 0.88. Similarly, the P_{fa}'s are 0.1 or 0.12. Note that there does not seem to be significant dependence on the distance from the radar, but that is because a slightly different symmetry criterion is used for ranges larger than 140 km. A more detailed examination of the symmetry criterion is in order because on a few occasions mesocyclones closer than 140 km also had a more elongated azimuthal shape and were thus classified as shears. Some misclassifications have been due to weak reflectivities below the thresholds, to imbalance of velocities (because of incorrect estimate of mesocyclone motion) and to poor velocity dealiasing.

False alarms were caused by incorrect velocity dealiasing and the presence of overlaid ground clutter or overlaid echoes from other storms. Often a mesocyclonic shear was split into two distinct features--some of these were false alarms and some were two genuine circulations. For instance, a

TABLE 9

Summary of Detection and False Alarm Probabilities

Date	Range (km)	P_d	Probabilities for the Day	
			P_d	P_{fa}
April 5, 1978	140 114 110 90	5/5=1 5/5=1 2/2=1 6/6=1	18/18=1	22/145=0.15
April 30, 1978	220 50	1/1=1 12/14=0.86	13/15=0.87	1/56=0.017
May 2, 1979	160-200 140-180 130-170 150	13/15=0.86 30/37=0.81 33/38=0.87 4/4=1	80/94=0.85	30/187=0.16
May 22, 1981	150 150 140 90-110 105 40-70	10/10=1 11/11=1 2/2=1 6/7=0.85 3/7=0.42 42/45=0.93	73/82=0.89	29/314=0.092

tornado vortex signature was identifiable as a separate feature, but was not always classified as M. From the available data, we deduced that TVS could be discriminated if a threshold on the average rotational speed of 15 $m \cdot s^{-1}$ and average shear of 20 $m \cdot s^{-1} \cdot km^{-1}$ is applied. Some reduction in false alarms is achievable if a feature with average shear less than 4 $m \cdot s^{-1} \cdot km$ or average moment less than 70 $m \cdot s^{-1} \cdot km^{-1}$ or average rotational speed less than 10 $m \cdot s^{-1}$ is classified as shear.

No attempt yet has been made to take full advantage of the quantitative estimates that the algorithm provides. That is, we have not related average rotational speed, momentum, etc., to the severity of damage produced by the mesocyclone. This should be done and will require a lengthy and careful examination of data and damage reports.

By no means have we optimized the various thresholds with respect to P_{fa} and P_d. Values for the momentum and shear thresholds (Table 1) are close to optimum. It should be sufficient to use one ratio of feature lengths which must be allowed to change beyond 120 km in order to accommodate for the azimuthal smearing. The minimum number of vectors M should be between 6 and 10; the maximum radial distance N should be 0.6 to 1.6 km; the maximum azimuthal distance R should be about 2°; and the average sum of beginning and ending velocities should be between 15 and 20 $m \cdot s^{-1}$. The reflectivity threshold of 15 dBZ is adequate. It is feasible to locate a decision boundary (i.e., set of thresholds that may depend on range) that maximizes P_d and minimizes P_{fa}. But before that is attempted, a more difficult problem is to obtain a unique description that characterizes a mesocyclone. Thus far, there has been no unique definition accepted by the community--neither in identifying mesocyclones nor in quantifying their severity. A certain amount of subjectivity is still necessary because not all the mesocyclone attributes are known. In marginal situations, which count quite a bit for detection probabilities, we found it difficult to be completely consistent.

5. Acknowledgments

Initially, the algorithm was developed by Larry Hennington; it was subsequently modified by Julie Skelton. Bill Bumgarner provided valuable guidance in the use of the Perkin Elmer computer on which the algorithm was run. Michelle Foster typed the manuscript, and Joan Kimpel drafted the figures.

APPENDIX

Effects of Smoothing by the Beam on the Ratio of Radial to Azimuthal Lengths

A viewing of an ideal Rankine combined vortex by a Doppler radar has been simulated on a computer (Zrnic' and Doviak, 1975). The simulation allows one to locate a resolution volume at a desired position with respect to the vortex center. Gaussian antenna pattern and range weighting functions are assumed, and the reflectivity of the vortex is assumed to be uniform. The simulation produces the Doppler spectrum and its moments corresponding to the location of the resolution volume. Of interest to us is the location of the maxima of mean velocities as a function of the azimuthal distance from the vortex center, because from these maxima one can obtain the maximum shears. Recall that it is the shear thresholds that determine if a candidate pattern vector will be saved for later sorting.

To illustrate the point, we have plotted on Fig. A.1 the location of velocity maxima and a curve on which the shear is constant ($\overline{v}\ r_t/v_m r\theta_1 = 0.3$). All variables are normalized to either radius, diameter or maximum velocity of the vortex, and it was assumed that the range extent of the resolution volume is $0.15 \cdot r_t$. Now let us consider a vortex with a 1-km radius and a 10 $m \cdot s^{-1}$ maximum rotational speed that is viewed by a radar whose beamwidth is 1°. At close ranges ($r < 10$ km) the azimuthal to radial length ratio (abscissa/ ordinate on Fig. A.1) is one.

Let us also assume that a pattern vector is detected when the shear threshold $\overline{v}/r\theta_1$ exceeds 3 $m \cdot s^{-1} \cdot km^{-1}$. Then at 60 km the ratio of the two lengths for this vortex is about 1.3 (not shown on figure), but at 120 km the ratio grows to 1.4 and at 156 km ($r\theta_1/D = 1.3$) it is 2.5. Thus, it is clear that the symmetry criterion must be amended at further ranges. We emphasize that besides range there are two more parameters that influence the shape of detected feature. These are the radius of maximum wind and the maximum rotational speed.

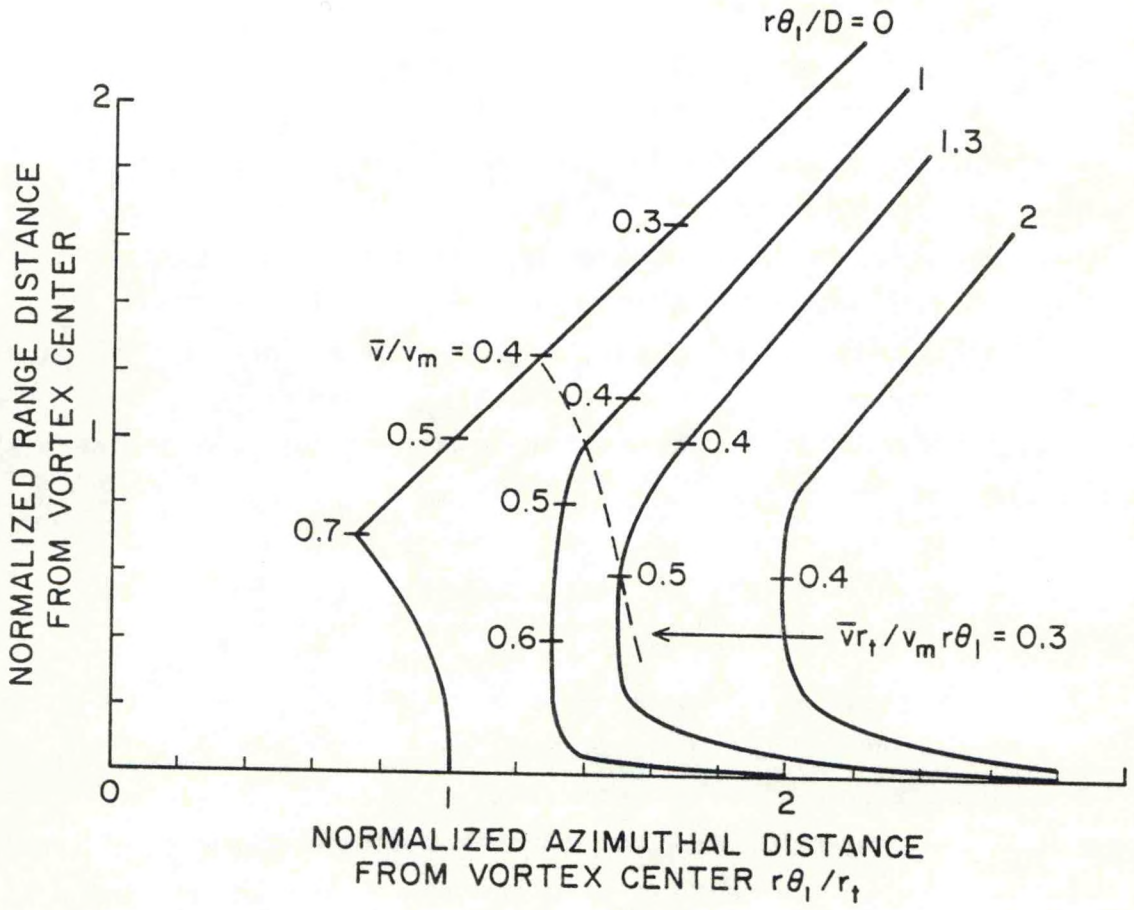

Figure A.1: Locations of the resolution volumes, which yield maximum mean velocities as a function of azimuthal distance from the vortex center. The range distance from the center (y axis) is the other independent parameter. Solid lines are for the indicated "beamwidth" $r\theta_1$ to vortex diameter D ratios. Tick marks signify the values of the normalized maximum mean velocity $\bar{v}$ to maximum rotational speed ratios. Dashed line corresponds to a constant normalized shear $\bar{v}r_t/v_m r\theta_1$ of 0.3 which is used in the illustrative example.

REFERENCES

Burgess, D.W., 1976: Single-Doppler radar vortex recognition: Part I - Mesoscale signatures. Preprints, 17th Conf. on Radar Meteor., Am. Meteor. Soc., Boston, Mass., 97-103.

Burgess, D.W., L.D. Hennington, R.J. Doviak, and P.S. Ray, 1976: Multimoment display for severe storm identification. J. Appl. Meteor., 15, 1302-1306.

Burgess, D.W., V.T. Wood, and R.A. Brown, 1982: Mesoscale evaluation statistics. Preprints, 12th Conf. on Severe Local Storms, Am. Meteor. Soc., Boston, Mass., 422-424.

Hennington, L.D., 1981: Reducing the effects of Doppler radar ambiguities. J. Appl. Meteor., 20, 1543-1546.

Hennington, L.D., and D.W. Burgess, 1981: Automatic recognition of mesocyclones from single Doppler radar data. Preprints, 20th Conf. on Radar Meteor., Am. Meteor. Soc., Boston, Mass., 704-706.

Joint Doppler Operational Project Staff 1979: Final Report on the Joint Doppler Operational Project (JDOP) 1976-1978. NOAA Tech. Memo., ERL NSSL-86, 84 pp.

Next Generation Weather Radar Algorithm Report, May 1983: Prepared by the NEXRAD Joint System Program Office.

Zrnic', D.S., and R.J. Doviak, 1975: Velocity spectra of vortices scanned with a pulse-Doppler radar. J. Appl. Meteor., 14, 1531-1539.

Zrnic', D.S., L.D. Hennington, and J. Skelton, 1982: Automatic recognition of mesocyclones from single Doppler radar data. Air Force Geophysics Laboratory report AFGL-TR-82-0291, October 1983.